Topological active matter

Suraj Shankar[1], *Anton Souslov*[2], *Mark J. Bowick*[3], *M. Cristina Marchetti*[4] *and Vincenzo Vitelli*[5,6,7] ✉

Abstract | In active matter systems, individual constituents convert energy into non-conservative forces or motion at the microscale, leading to morphological features and transport properties that do not occur in equilibrium and that are robust against certain perturbations. In recent years, a fruitful method for analysing these features has been to use tools from topology. In this Review, we focus on topological defects and topologically protected edge modes, with an emphasis on the distinctive properties they acquire in active media. These paradigmatic examples represent two physically distinct classes of phenomena that are robust thanks to a common mathematical origin: the presence of topological invariants. Beyond active matter, our Review underscores the role of topological excitations in non-equilibrium settings of relevance, from open quantum systems to living matter.

A variety of media can be regarded as active matter, that is, out-of-equilibrium systems composed of individual components that convert energy into non-conservative forces and motion at the microscale[1–3]. Examples include self-propelled particles, such as micron-sized colloids powered by chemical reactions[4,5], biofilaments with molecular motors[6,7] and biological systems ranging from epithelial tissues and bacterial colonies to bird flocks[8–10]. Describing these media using continuum equations, as one would for passive fluids or solids, requires a careful re-examination of the symmetries and conservation laws that are present (or, indeed, absent) in each active system[2]. The most obvious example is the conservation of energy, which is manifestly violated by the presence of molecular motors or other mechanisms of energy transduction at the microscale that power self-sustained flows and active stresses. This energy injection at the microscale is responsible for morphological features and transport properties that do not occur in equilibrium and that are robust against certain perturbations. Some of these robust features have been fruitfully analysed using the tools of topology.

Topology describes properties of objects that are preserved under continuous deformations of their shapes. A common example is the smooth deformation of a doughnut into a mug. During this transformation, the shape of the object changes but the number of holes, s, is preserved, as long as the material is not torn or glued together. The integer s, called the genus, is an example of a topological invariant. In condensed matter physics, a prime application of topological invariants is in the characterization of topological defects, which are particle-like objects that describe global deformations of an ordered medium[11–13]. For example, a system of elongated molecules lying in a plane can be described by a 2D vector field. An isolated vortex (BOX 1) in the field can be parameterized by the position of its centre — it is a particle-like object. However, its presence disrupts molecular alignment throughout space — the deformation is global.

The global character of a vortex is captured mathematically by the definition of its winding number. The local angle that the molecules make with respect to a fixed direction in the plane can be described by the field $\theta(\mathbf{r})$ (that is, the vector order parameter). The winding number, s, is then an integer that tracks the cumulative change in $\theta(\mathbf{r})$ along any path enclosing the vortex:

$$s = \frac{1}{2\pi}\oint \nabla\theta \cdot \mathrm{d}\mathbf{l}. \qquad (1)$$

Much like how the number of holes on a surface is preserved under continuous deformations of its shape, the integer s is also a topological invariant. The only difference is that, in this case, s is preserved under continuous deformations of the vector order parameter. As a result, a vortex characterized by the non-vanishing winding number $s = 1$ is said to be topologically stable or robust: it cannot be made to disappear ($s \to 0$) unless annihilated with a topological defect characterized by a winding number of opposite sign, that is, an anti-vortex (BOX 1). Note that, if the line integral in Eq. (1) is evaluated along a path that encircles multiple vortices and anti-vortices, s measures the net number of topological defects (to which a positive or negative sign is assigned, depending on their individual winding numbers).

A similar mathematical mechanism ensures the robustness of so-called chiral edge modes in topological

[1]*Department of Physics, Harvard University, Cambridge, MA, USA.*
[2]*Department of Physics, University of Bath, Bath, UK.*
[3]*Kavli Institute for Theoretical Physics, University of California, Santa Barbara, Santa Barbara, CA, USA.*
[4]*Department of Physics, University of California, Santa Barbara, Santa Barbara, CA, USA.*
[5]*James Franck Institute, The University of Chicago, Chicago, IL, USA.*
[6]*Department of Physics, The University of Chicago, Chicago, IL, USA.*
[7]*Kadanoff Center for Theoretical Physics, The University of Chicago, Chicago, IL, USA.*
✉*e-mail: vitelli@uchicago.edu*

https://doi.org/10.1038/s42254-022-00445-3

Key points

- Topology plays a defining role in understanding robust features in active media whose basic constituents convert energy into non-conservative forces and motion.
- Topological defects in active media can acquire self-propulsion and non-reciprocal interactions.
- Local stresses and flows generated by active defects can have biological functionality in living systems.
- When detailed balance is broken, unidirectional density waves emerge that are protected against scattering by the presence of topological invariants in the band structure of the media.
- Non-Hermitian band theory naturally arises in active materials because energy is both consumed and dissipated, resulting in the presence of skin modes and odd viscoelasticity.
- The full potential of these ideas extends from the fundamental understanding of topology in non-equilibrium systems to applications including materials design and tissue mechanics.

insulators[14–17]. These are waves that propagate unidirectionally along sample boundaries without experiencing any backscattering, even if they encounter sharp corners or obstacles on their way[18,19]. This property can be traced to the presence of a topological invariant called a Chern number[20]. This integer, which we denote by $\mathcal{C}$, measures the net number of unidirectional — that is, chiral — edge modes present. The Chern number is positive or negative, depending on whether the modes propagate clockwise or counterclockwise. Chiral edge modes are topologically robust, much like the vortices discussed above. In this case, the Chern number (and, hence, the very presence of an edge mode) is preserved under continuous changes in the physical parameters, such as lattice geometry (rather than under continuous deformations of the order parameter). On a more technical level, topological invariants, such as Chern numbers, can also be viewed as winding numbers encircling topological defects, but in wave vector space, as discussed in this Review.

Topological defects and topologically protected modes (such as chiral edge states) are intertwined[21–24]. In addition to boundaries, topological modes can be localized around defects such as vortices, dislocations or domain walls. Topological defects[11,13,25] and topologically protected modes[26–31] occur in a variety of physical contexts, but in active media they acquire distinctive properties, which are the focus of this Review.

Active media display non-conservative stresses and spontaneous flows, and, therefore, they naturally break key symmetries that passive materials would possess[2,3]. For example, active media can violate reciprocity[32,33] and detailed balance[34,35]. Non-equilibrium violations of either of these principles introduces an arrow of time and enables the presence of non-vanishing currents (of energy, momentum or particles) in the steady state of active systems. In turn, these currents endow topological modes and defects with properties absent at equilibrium and, in some cases, enable their very existence. We illustrate this point with two examples.

First, topological defects (which normally cost a large elastic energy[25]) can unbind and proliferate even at zero temperature if active stresses are present[36,37]. This unbinding occurs in active nematics[38,39], which are liquid-crystalline media composed of, for instance, cytoskeletal filaments driven by molecular motors[7,40]. Moreover, the resulting topological defects can move by themselves, that is, even in the absence of external forces or fields[7,41,42]. This spontaneous 'self-propulsion' depends on the winding number of the defects[42] (such that defects with a positive winding number can self-propel) and ultimately originates from the presence of non-conservative internal forces generated by adenosine-triphosphate-powered molecular motors on the microscale.

Second, chiral edge modes occur in mechanical, optical and electronic systems[15,26–31], but, in the simplest situation, external fields (for instance, applied magnetic fields) are typically required to break the symmetry between left-moving and right-moving waves. A simple way to break this symmetry in mechanics is to build a lattice of circulators[43,44]. Experiments[43,44] reveal that, when many such circulators are assembled into a lattice, the sound waves propagating on top of the flowing fluid are topologically protected. If one now fills the rings with self-propelled particles (instead of a passive fluid like air), the required flow arises spontaneously without motorizing the circulators: the microscopic particles themselves are motorized[45]!

In this Review, we build on the examples considered above and provide an introduction to the theory of topological active matter and a survey of its rich experimental ramifications. We first explain the mechanisms whereby topological defects self propel and proliferate in active nematics, leading to collective states that can be manipulated by geometry and patterning. Possible implications for active microfluidics and biological tissues are presented. We then illustrate how the propagation of waves in active fluids and solids is affected by the presence of topological invariants that characterize their dispersion relations. We discuss the relevance of these ideas for the design of robotic metamaterials and the properties of active granular and colloidal systems.

Topological defects in active matter

In passive materials, topological defects are inevitably formed when the system is quenched from the disordered into the ordered state, or when order is frustrated by curvature, external fields or boundary conditions. Topological defects constitute elementary excitations of the homogeneous ordered state and their statistical mechanics offers a picture dual to that of the familiar order parameter[13]. Order–disorder transitions in many passive 2D systems, including superfluid and superconducting films, crystalline layers and 2D nematics, are controlled by the unbinding of topological defects through the superfluid-like Berezinskii–Kosterlitz–Thouless (BKT) mechanism[46–50]. The BKT theory reveals a distinct universality class of defect-induced continuous phase transitions at equilibrium[50]. The theory relies on mapping the statistical physics of point defects onto a gas of interacting Coulomb charges. At low temperature, opposite-sign defect pairs are bound by Coulomb-like attraction and the state remains ordered. Above a critical temperature, entropic effects overcome energetic

Reciprocity
The symmetry between perturbation and response.

Detailed balance
The symmetry between the past and the future within the dynamics of microscopic processes.

Circulators
A ring in which air is constantly moved by a fan.

Metamaterials
Materials with properties arising from their macroscopic structure, rather than their chemical constituents. A simple example is a 'holey sheet': a slab of rubber with holes that have size and shape tailored to achieve a specific mechanical response.

attraction, resulting in defect unbinding, which destroys the ordered state[13,25].

Likewise, defects play an important role in the spatiotemporal dynamics and relaxation of active ordered phases. We focus here on orientationally ordered fluids, which can host point-like defects in 2D, and both point-like defects (monopoles, also called asters) and line-like defects (disclinations) in 3D (REFS[11,12]). One class of such active ordered fluids is polar active fluids, also called Toner–Tu fluids[51–54]. These collections of polar active particles with aligning interactions, akin to 'flying spins', can order in states characterized by collective motion, in which the order parameter is the mean velocity of the flock (TABLE 1). In such polar active fluids, the ordered state is a state of mean motion that spontaneously breaks rotational symmetry and time-reversal symmetry (TRS) on a global scale. Another class of orientationally ordered fluids is active nematics[38,39], which are composed of head–tail symmetrical rod-like entities that exert internally generated stresses on their surroundings and organize in states of orientational order that is apolar. These fluids display no net motion on average, but combine the rich rheology of liquid crystals with active driving. TABLE 1 describes some commonly used continuum models to describe such systems.

Active ordered fluids have been assembled from a variety of soft materials[5–7,55,56]. The orientationally ordered state becomes unstable on length scales L when the active stresses (see TABLE 1) exceed elastic stresses $\sim K/L^2$ (REF.[57]), where K is the stiffness. Bulk ordered states ($L \to \infty$) are, therefore, unstable for any amount of activity, but can be stabilized below a critical value of activity by confinement[58] or friction with a substrate[59]. At large activity, all liquid-crystalline active fluids display turbulent-like dynamics with a proliferation of topological defects. Polar fluids with vectorial order parameters

Box 1 | Topological defects in passive and active ordered fluids

Topological defects are special zeros of the order parameter field. They are point-like in 2D liquid-crystalline media and are classified by their winding number or topological charge $s = \Delta\Theta/2\pi$ (also see Eq. (1)), where $\Delta\Theta$ is the net angle through which the order parameter rotates as one encircles the defect. The charge ν is positive if the order parameter rotates in the same direction as the path traversed and negative if it rotates in the opposite direction. In a 2D XY magnet, the order parameter is a vector field and the lowest-charge topological defects are asters and vortices (both with $s = +1$), and anti-vortices or cross hairs (with $s = -1$), as shown in part **a** of the figure. In a nematic film, the broken symmetry identifies only orientation (not direction) and the order parameter is a line field, and the lowest energy defects are disclinations with $s = \pm 1/2$ (part **b** of the figure).

In 2D passive liquid crystals, two defects of strength s_i and s_j and separation $\mathbf{r}_{ij}$ interact via a Coulomb potential, mediated by nematic elasticity (K) and cut off by the defect core size (a):

$$V(\mathbf{r}_{ij}) = 2\pi K s_i s_j \ln\left(\frac{|\mathbf{r}_{ij}|}{a}\right)$$

In 2D active nematics, defects behave like quasiparticles 'dressed' by the active flows they produce[36,39,42]. Such a description is appropriate deep in the nematic regime, where the defect core size (a) is the smallest length scale in the system. The flow generated by a +1/2 defect is finite at the core, rendering the defect a self-propelled particle with a well-defined polarization ($\mathbf{e}_i$), as shown in part **d** of the figure. On the other hand, the flow generated by a −1/2 defect vanishes at the core. To leading order in activity, defects interact via the same Coulomb force as in the passive case but also exert active torques on each other. Defects in active nematics, therefore, behave as an interacting mixture of active (+1/2) and passive (−1/2) charged quasiparticles[36].

Defects with $s = -1/2$ generate a flow that vanishes at their core and are, thus, passive particles to leading order in activity; defects with $s = +1/2$ generate a flow that is finite at their core, rendering them self-propelled particles with velocity $v_{core} \sim |\alpha|$, where α is the strength of the active stresses (part **c** of the figure)[36,39,42].

Bulk active nematics support topologically neutral disclination loops that smoothly interpolate +1/2 and −1/2 defect textures in local cross sections of the loop. The ±1/2 wedges are equivalent in 3D by escape into the third dimension. The simplest of such wedge–twist (W–T) loops is characterized by a rotation vector (**Ω**) in the plane of the loop ($\gamma = \pi/2$), making an angle β with the local tangent (**t**) (see part **e** of the figure). Like their 2D counterparts, such disclination loops generate local active flows that drive complex dynamics in 3D bulk active nematics[87].

Figure part **d** adapted with permission from REF.[37]. Figure part **e** adapted with permission from REF.[87].

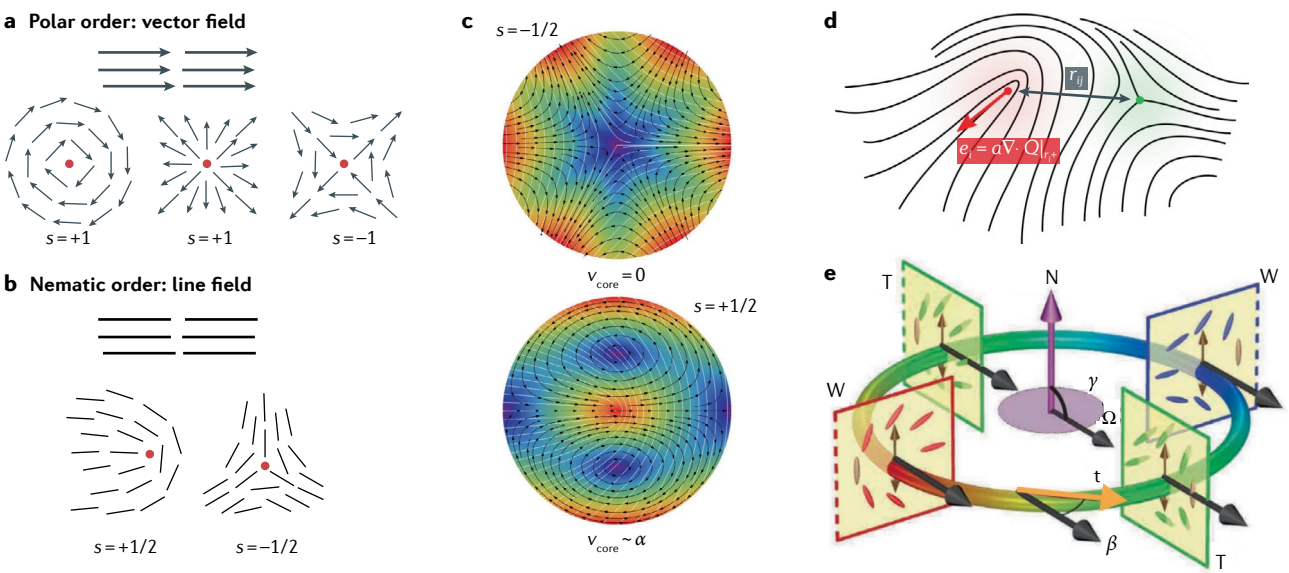

Table 1 | **Models of active fluids**

System	Particles	Order parameter	Example model	Model notes
Active polar fluids, such as polar fluid composed of colloidal rollers 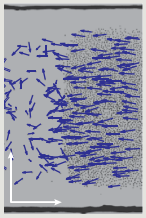	Polar: self-propulsion speed v_0 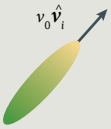	Collective polar order: vector order parameter $\mathbf{P} = \langle \sum_i \hat{\nu}_i \delta(\mathbf{r} - \mathbf{r}_i) \rangle$ 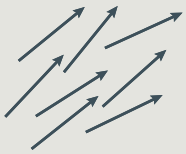	Toner–Tu equations[52,53]: $\partial_t \rho + v_0 \nabla \cdot (\rho \mathbf{P}) = 0$, $\partial_t \mathbf{P} + \lambda \mathbf{P} \cdot \nabla \mathbf{P} = [a_2 - a_4 \lvert \mathbf{P} \rvert^2]\mathbf{P} + K\nabla^2 \mathbf{P} - \nabla \Pi$	v_0 and λ are active parameters capturing advection; a_2 and a_4 control the ordering transition; K is an elastic constant; and $\Pi(\rho)$ a density-dependent pressure
Active nematic fluids, such as a microtubule–kinesin film 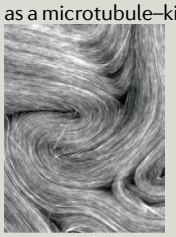	Apolar: exerts force dipole $\alpha \sim f\ell$ 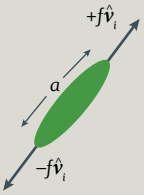	Nematic order: tensor order parameter (in d dimensions) $\mathbf{Q} = \langle \sum_i (\hat{\nu}_i \hat{\nu}_i - \frac{1}{d}) \delta(\mathbf{r} - \mathbf{r}_i) \rangle$ 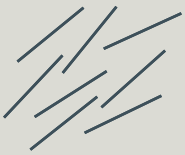	Incompressible hydrodynamics of nematic order ($\mathbf{Q}$) coupled with flow ($\mathbf{u}$) driven by an active stress ($\sigma_a = \alpha \mathbf{Q}$)[39]: $\partial_t \mathbf{Q} + \mathbf{u} \cdot \nabla \mathbf{Q} + [\omega, \mathbf{Q}] = \lambda \mathbf{E} + [a_2 - a_4 S^2]\mathbf{Q} + K\nabla^2 \mathbf{Q}$, $\eta \nabla^2 \mathbf{u} - \Gamma \mathbf{u} + \nabla \cdot \sigma_a - \nabla \Pi = \mathbf{0}$, $\nabla \cdot \mathbf{u} = 0$	Force balance involves friction (Γ), viscosity (η) and pressure (Π); $\mathbf{E}$ and ω are the symmetric and antisymmetric parts, respectively, of the strain rate tensor ($\nabla \mathbf{u}$); λ is the flow alignment parameter; nematic ordering [$S^2 = \mathrm{tr}(\mathbf{Q}^2) d/(d-1)$] is controlled by a_2 and a_4; and K is the elastic stiffness
Scalar active matter 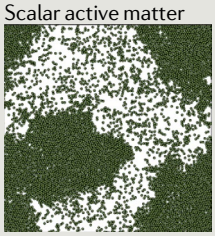	Scalar active particle with no alignment 	Phase separation: scalar order parameter, the density difference between liquid (ρ_L) and gas (ρ_G) phases $\rho = \langle \sum_i \delta(\mathbf{r} - \mathbf{r}_i) \rangle$, $\phi = \frac{(2\rho - \rho_L - \rho_G)}{(\rho_L - \rho_G)}$ 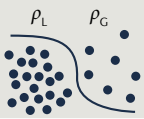	Motility-induced phase separation described by Cahn–Hilliard dynamics involving the density (ρ)[253]: $\partial_t \rho = \nabla \cdot [D(\rho) \nabla \mu]$, $\mu = \ln[\rho v(\rho)] + \kappa(\rho) \nabla^2 \rho$	The effective chemical potential μ includes the density suppression of motility $v(\rho)$ and nonintegrable gradient terms ($\kappa'(\rho) \neq 0$); density also suppresses the diffusion constant ($D \propto [v(\rho)]^2$)
Chiral active fluids, such as colloidal spinning magnets 	Chiral active particle self-spinning at rate Ω_i in 2D 	Collective chirality: scalar field, the intrinsic rotation frequency $\Omega = \langle \sum_i \Omega_i \delta(\mathbf{r} - \mathbf{r}_i) \rangle$ 	Hydrodynamics of an isotropic chiral active fluid in 2D, including density (ρ), flow ($\mathbf{u}$) and the internal spin density (Ω)[168,175]: $\partial_t \rho + \nabla \cdot (\rho \mathbf{u}) = 0$, $\partial_t \mathbf{u} = \eta \nabla^2 \mathbf{u} - \Gamma \mathbf{u} + \eta_R \nabla_\perp (2\Omega - \omega) + \eta_o \nabla^2 \mathbf{u}_\perp - \nabla \Pi$, $\partial_t \Omega = \tau_0 - \Gamma_\Omega \Omega - 2\eta_R (2\Omega - \omega) + D_\Omega \nabla^2 \Omega$	Besides regular viscosity (η) and friction (Γ), odd viscosity (η_o) and rotational viscosity (η_R) are also present, the latter in the antisymmetric stress; chirality enters through terms involving $\mathbf{u}_\perp = \hat{\mathbf{z}} \times \mathbf{u}$ and the vorticity $\omega = \hat{\mathbf{z}} \cdot (\nabla \times \mathbf{u})$; the active torque ($\tau_0$) injects spin into the fluid, which is damped by spin friction (Γ_Ω) and diffusion (D_Ω)

f, active force; ℓ, particle length; $\hat{\nu}_i$, orientation or direction of propulsion of particle i. Polar fluids image adapted from REF.[5], Springer Nature Limited. Nematic fluids image adapted from REF.[7], Springer Nature Limited. Scalar active matter image adapted with permission from REF.[252]. Chiral fluid image adapted from REF.[170], Springer Nature Limited.

exhibit defects that are characterized by an integer topological charge, such as vortices and asters. In contrast, the inversion symmetry of nematic order means that the order parameter maps onto itself after a winding of only 180° around the defect core (the small, roughly circular, region of space that surrounds the defect centre and in which the nematic order parameter vanishes). Thus, defects with half-integer charge known as disclinations (TABLE 1) are allowed. Because the energetic cost of a defect is proportional to the square of its charge, ±1/2 disclinations are the lowest-energy defects in nematics; they are not allowed in polar (vector) fluids. The presence of ±1/2 defects, therefore, provides a fingerprint of the apolar nature of the broken symmetry and a criterion for distinguishing nematic from polar order.

Asters and vortices have been observed in high-density motility assays[60,61], confined and membrane-bound reconstituted cortical extracts[55,56,62] and suspensions of colloidal rollers motorized by an electric field[63]. Nematic disclinations have been identified in systems including cytoskeletal filament-based active nematic suspensions[7,40,64,65], collections of living cells[66–72] and even multicellular organisms[73]. In recent years, topological defects have been the focus of intensive research, particularly in active nematics[39]. Such systems exhibit self-sustained and spatiotemporally chaotic large-scale flows accompanied by the spontaneous proliferation of topological defects. It is, therefore, natural to ask whether the chaotic dynamical state of active nematics can be understood from the perspective of defect

Colloidal rollers
Micron-sized dielectric spheres suspended in an ionic solvent that can undergo an electrohydrodynamic instability (Quincke instability), causing the spheres to spontaneously roll upon the application of a strong enough DC electric field.

unbinding and whether the equilibrium BKT transition has an analogue in the active realm.

In both passive and active liquid crystals, distortions of orientational order generate flows, and flows, in turn, deform the ordered state. The key distinction between passive and active systems is that, in passive systems, flows and deformations are generated by applying external fields or via boundary conditions. Such flows are transient: the system always relaxes to the equilibrium (ordered) state upon removal of perturbations or constraints. In active systems, by contrast, flows and deformations are internally generated and self-sustained. In 2D, bulk active nematics are generically unstable to bend or splay deformations generated by local active fluctuations[57]. As these distortions grow in time, they generate flows that further enhance the deformations, ultimately generating unbound pairs of topological defects. Such spontaneously generated defects are themselves strong distortions of orientational order and yield distinctive flow patterns[42,74]. This intimate connection between defects and flows offers the opportunity to direct and localize nonlinear active flows by controlling the dynamics of topological defects[37,75,76]. There is evidence that biological systems may exploit this connection between structure and dynamics, and use defects to localize stresses and perform specific biological functions[71–73,77–80]. These subjects are the focus of the rest of this section.

Spontaneous motion of active defects. One of the distinguishing aspects of defects in active matter is their capacity for spontaneous and autonomous motion. The large distortions of the order parameter around a topological defect generate local active flows, the symmetry and profile of which are controlled by the defect geometry. In particular, in 2D active nematics, the comet-like +1/2 defect (BOX 1) generates a flow that is finite at the defect core. The +1/2 defect then rides along with the flow it generates, behaving like a self-propelled polar particle[42,81]. In contrast, the flow generated by a −1/2 defect vanishes at the defect core, owing to the defect's threefold symmetry (BOX 1), and to leading order in activity, such a defect remains a 'passive' particle. The direction of motion of the +1/2 defect is determined by its local orientation or polarity and by the sign of the active forcing. Active stresses that cause material extension along the ordering axis are called 'extensile', whereas those that contract along the same axis are called 'contractile'. In extensile fluids, +1/2 defects actively propel themselves along the head of the comet, while in contractile systems, the active propulsion is directed along the comet's tail. If chiral active stresses are present, +1/2 disclinations self-propel instead at an angle relative to their polarity[82,83], and intrinsic active spinning renders defect trajectories circular[82]. In polar fluids, spiral vortices of charge +1 undergo spontaneous rotation[84] owing to the chirality of their spiral texture. Other low-charge defects, such as circularly symmetrical asters and anti-vortices, perform neither rotational nor translational spontaneous motion. In contrast to defect motion in externally driven systems, the motion of active defects is dictated by the local geometry of the defect itself and not by a fixed external field, as would be the case, for example, for driven vortices in a superconducting film. This profound distinction leads to a plethora of phenomena characteristic of active matter.

Defects can also occur in 3D active suspensions, but they are less well understood. As in 2D, bulk active nematics in 3D are susceptible to a generic hydrodynamic instability[57] that spontaneously generates individual charge-neutral disclination loops[85–88] (BOX 1). Unlike in 2D, where topological charge conservation constrains point defects to be created and annihilated in pairs of opposite charge, in 3D, charge-neutral disclination loops[12] can be nucleated on their own. The active flows caused by the director distortion around such a disclination loop cause it to stretch, twist and buckle[88]. The complex configurational dynamics of these loops combined with topological reconnections leads to chaotic 3D flows that have been observed in simulations[85,86] and experiments[87]. Similar ideas have been extended via theoretical work to chiral phases such as bulk active cholesterics[89–91]. In the case of cholesterics, λ-lines, which are defects in the cholesteric pitch with no director singularity at their core[89], and other nonsingular topological textures called half-skyrmions or merons[90] can sustain coherent rotations and steady defect patterns along with spatiotemporal chaotic flows, even though these defects are not self-propelled.

Defect dynamics, unbinding and ordering out of equilibrium. From a fundamental point of view, defect motility raises intriguing possibilities for phase transitions. The consequences of defect self-propulsion have been explored predominantly in 2D active nematics[36,37,42,74,81,92]. The defect-driven chaotic flows lead to a state dubbed 'active turbulence'[74,93], which is characterized by vorticity and shear flows on a typical length scale that controls the mean defect separation and is set by a balance of active and elastic stresses[68,74,94–96]. The phenomenology and scaling properties of active turbulence have been reviewed in recent years[39,97]. Here, we focus on the topological aspects of active turbulence and sketch the physical arguments underpinning the unbinding of active defects[36].

In passive liquid crystals, defects in 2D behave as point charges that interact via a Coulomb potential. This pair interaction is mediated by the underlying elasticity of the ordered fluid and scales as $K\ln(r/a)$, where r is the pair separation and a the defect core size (TABLE 1). In a 2D active nematic, an isolated ±1/2 disclination pair continues to experience the passive attractive force $\sim K/r$ from elasticity, but, in addition, for certain configurations, such as that shown in BOX 1, the +1/2 defect can propel itself with speed $\sim v_0$ away from the −1/2 defect. The balance of elastic and active forces sets a length scale $r_c \sim K/v_0$, beyond which activity always rips apart the defect pair, causing it to inevitably unbind. This simple picture is spoiled by the fact that +1/2 defects do not travel in a straight line. Instead, their direction of motion is affected by rotational noise and changes in the local nematic structure. Because the motility of +1/2 disclinations is determined by their local geometry, the +1/2 defect has a finite persistence length $\ell_p = v_0\tau_R$,

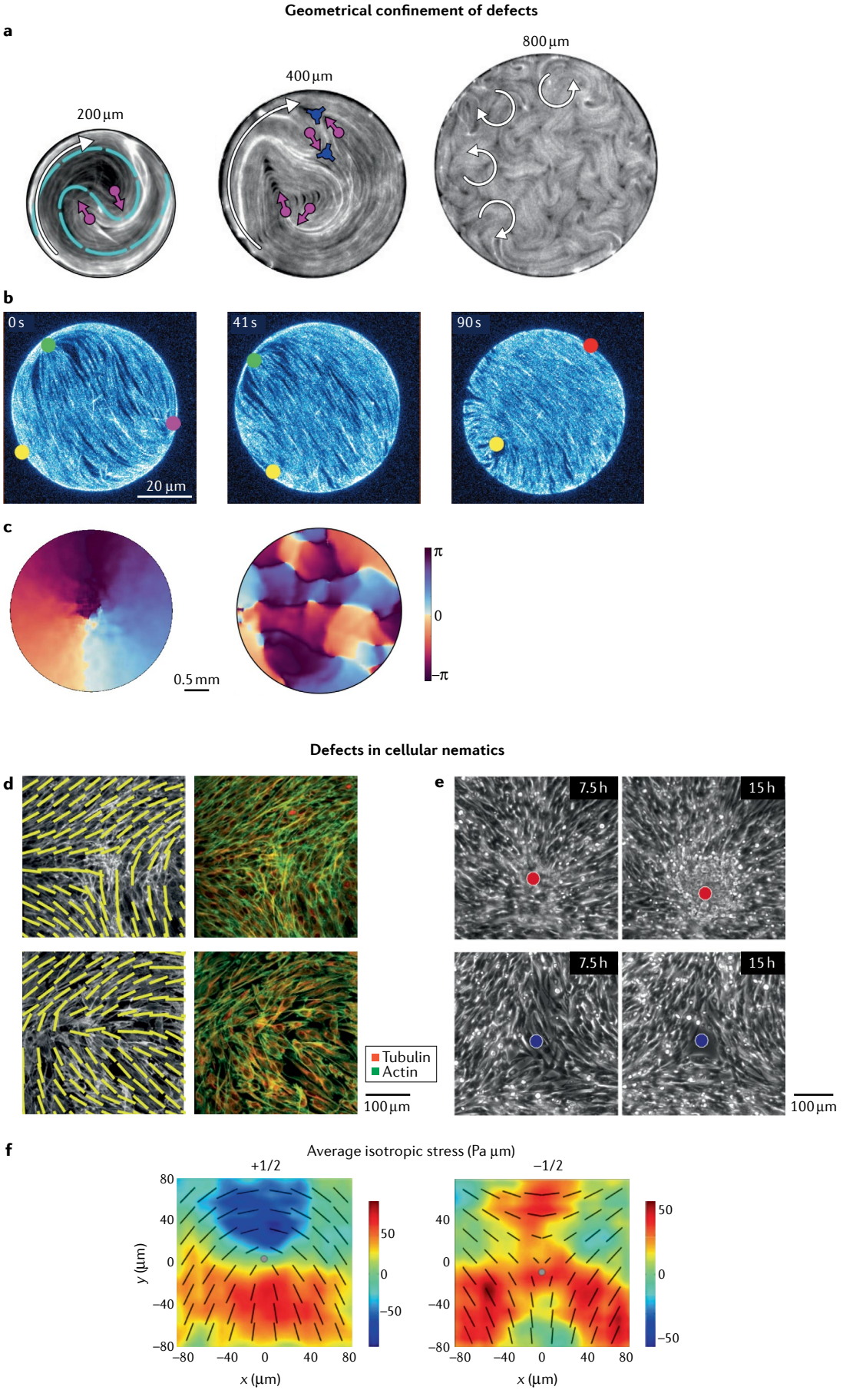
Geometrical confinement of defects
a
200 µm
400 µm
800 µm
b
0 s
41 s
90 s
20 µm
c
π
0
–π
0.5 mm
Defects in cellular nematics
d
e
7.5 h
15 h
7.5 h
15 h
Tubulin
Actin
100 µm
100 µm
f
Average isotropic stress (Pa µm)
+1/2
–1/2
80
40
0
–40
–80
y (µm)
–80 –40 0 40 80
x (µm)
50
0
–50
40
0
–40
–80
–80 –40 0 40 80
x (µm)
50
0
–50

◀ Fig. 1 | **Dynamics of defects under confinement. a**,**b** | Geometrical confinement of defects. Circulating +1/2 defects in a microtubule–kinesin active nematic film confined to a disc (200 μm), with more pairs of defects unbinding to create turbulent flows for large disc diameters (800 μm) (part **a**); the same system now condensed onto a spherical vesicle exhibits periodic oscillations of the four +1/2 defects present (part **b**). **c** | Schlieren texture of a colloidal polar fluid in a disc geometry displaying a system-spanning vortex (left) and a pattern of pinned vortex–anti-vortex pairs (right) induced by randomly located obstacles[115]. **d** | Active ±1/2 disclinations have been identified in aligned populations of spindle-shaped mouse fibroblasts. **e**,**f** | Cells accumulate at the cores of +1/2 defects and deplete at the cores of −1/2 defects (part **e**). The +1/2 defects seed mound formation in dense monolayers of neural progenitor cells. Similar defects in epithelial monolayers of Madin–Darby canine kidney (MDCK) cells (part **f**) generate large compressive stresses (in blue) only at the head of +1/2 disclinations that locally trigger cell extrusion and apoptosis[71]. Part **a** adapted with permission from REF.[126]. Part **b** adapted with permission from REF.[64]. Part **c** adapted with permission from REF.[115]. Part **d** adapted from REF.[69], Springer Nature Limited. Part **e** adapted from REF.[72], Springer Nature Limited. Part **f** adapted from REF.[71], Springer Nature Limited.

beyond which its motion is not ballistic, where τ_R^{-1} controls the rate of rotational noise from active processes. Comparing this persistence length with the length scale r_c at which pair attraction and defect propulsion balance yields a simple criterion for active defect unbinding[36]. Defect pairs unbind if $\ell_p > r_c$. Conversely, when $\ell_p < r_c$, the +1/2 defect changes its direction of motion before overcoming Coulomb attraction, resulting in a local change of the nematic texture that allows the pair to remain bound. It is interesting to note that, in this situation, the rotational noise stabilizes the quasi-ordered nematic phase below a finite activity threshold by disrupting the persistent motion of the +1/2 defect. This order-from-disorder mechanism highlights the difference between active and driven defects: in purely driven systems, the latter inevitably unbind under the action of any external field because nothing disrupts their straight line motion.

Above a critical value of activity, the BKT-like unbinding yields an interacting gas of unbound defects that swarm. This gas provides a useful picture to describe the state of active turbulence. Several models of varying complexity have been proposed for the dynamics of active defects[36,42,64,81,98–102]. Although details differ, the basic physics is the same: the unbound defect gas is a mixture of self-propelled (the +1/2 defects) and passive (the −1/2 defect) charged particles that interact via Coulomb forces. More recent work has also emphasized the non-reciprocal nature of active defect interactions[102,103], although its detailed consequences remain to be explored. Coarse-graining over many defects allows a hydrodynamic description of the active defect gas[37,104], along the lines of previous classic works in the context of superfluid vortices[105] and 2D crystal melting[106]. Importantly, a hydrodynamic treatment of defects offers a theoretical handle on the strongly interacting many-body dynamics of this far-from-equilibrium system.

As a crucial ingredient, this description includes a polarization field that captures the average orientation of a collection of active +1/2 defects. This field accounts for self-propulsion actively driving material flow; furthermore, being a vector, the orientation of the field also experiences active torques. When activity is sufficiently strong, and viscous stresses are negligible compared with frictional dissipation with a substrate, the +1/2 defects spontaneously condense into a polar-ordered collectively moving state — a defect flock[37]. The fleeting defects constantly turn over owing to creation and annihilation events, but polar order persists for infinitely longer than the individual defect lifetime. Heuristically, such a state arises when the underlying nematic elasticity is too slow to relax the distortion created in the wake of an unbinding defect pair. Similar defect-ordered states have been observed previously in simulations, either with polar ordering[107–110] or defect lattices[111]. In addition, a nematic ordered defect state has been observed in experiments on active nematic films consisting of microtubules and kinesin[107]. Although continuum simulations recover largely transient nematic defect ordering[109,112], this observation continues to be a theoretical puzzle. Work published in 2020 suggests that elastic torques may play a role in antipolar ordering of defects[113,114].

Finally, vortex unbinding has been shown to also play a role in disordered polar active fluids[115]. In such fluids, active flows conspire with quenched obstacles to realize a dynamic vortex glass that can be explained through an effective BKT-like argument, in analogy with dirty superconductors. How to generalize similar ideas to active matter in heterogeneous environments[116] remains an open question.

Active defects under confinement. The direct connection between defects and active flows offers new avenues for rectifying and controlling the spontaneous chaotic dynamics of active nematics (FIGS 1,2). Doing so would pave the way to develop active microfluidic devices using these systems[117]. Active nematic films built by depleting microtubule bundles and kinesin motor complexes onto an oil–water interface[7] have emerged as a versatile platform to manipulate defects by controlling the material properties and structure of the supporting interface. One simple approach for such control is to tune the viscosity of the oil layer that hydrodynamically constrains the nematic flow[118]. Other techniques involve using more structured environments that can be controlled by external fields and themselves patterned with defects, such as by using bulk smectics as a substrate for active nematics[95,119] (FIG. 2b). For example, when in contact with the active nematic layer, focal conic domains in the smectic cause the active disclinations to swirl along circular trajectories[95]. In 3D, active drops in a passive nematic fluid can also entrain and activate the dynamics of passive defects, such as ring disclinations in the surrounding nematic[120,121]. These methods provide a neat way to rapidly reconfigure and channel flows in the system by rectifying defect motion.

Physical confinement has also been studied, particularly in the disc geometry. Spiral vortices were first stabilized in bacterial suspensions by confinement[122,123], although their size was limited ($\lesssim$80–100 μm) by their intrinsic instability towards turbulence. High solvent viscoelasticity can 'calm' active turbulence and allow larger, millimetre-scale bacterial vortices that exhibit both coherent and globally oscillating flows[124]. Another example is polar fluids of colloidal rollers, which lack

Smectics
Describes a type of liquid crystal in which molecules order in periodic layers; each layer behaves like a fluid in its plane.

Focal conic domains
Characteristic defects seen in smectic liquid crystals. They occur when equidistant layers of the smectic form geometric structures consisting of nested surfaces generated by conic sections, the foci of which lie on a curve given by the conjugate conic section.

the hydrodynamic interactions that cause bacterial turbulence. These fluids self-organize into a macroscopically stable vortex pattern when confined to circular tracks[63]. They also exhibit states consisting of pinned vortices in the presence of quenched disorder in the substrate[115] (FIG. 1c). Another system that develops steady circulating flows when strongly confined to discs is microtubule-based active nematics, though, in these, the steady flow is driven by a pair of +1/2 defects (as topologically required) that nucleate at the boundary and orbit around each other[125,126]. For large disc sizes, more defects nucleate and unbind in the bulk, degenerating into active turbulence (FIG. 1a). Finally, laterally confined nematics support shear states into which +1/2 defects are continually injected, as the defects swim around each other in a dancing fashion[127,128]. Although experiments and continuum simulations agree well in many regards, there are discrepancies in predictions related to defect nucleation and steady flow states in confined nematics[126], suggesting that more theoretical work is required.

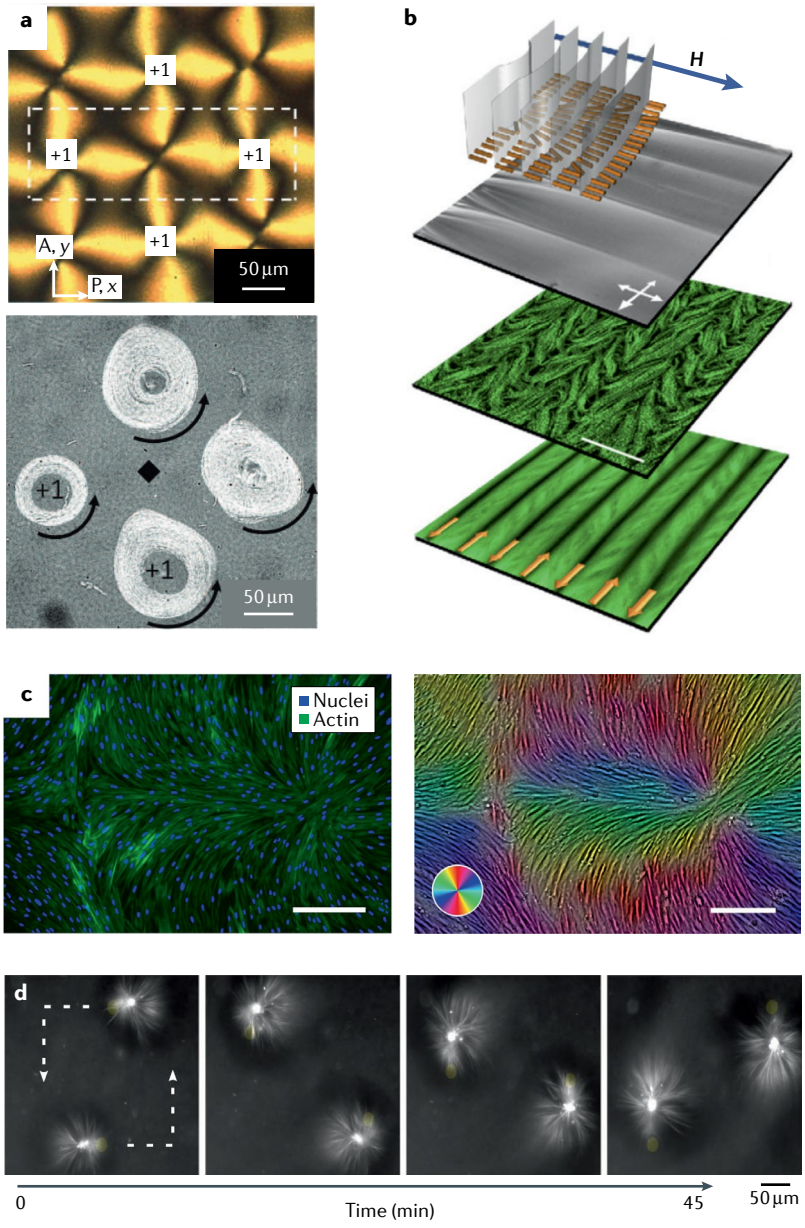

Fig. 2 | **Controlling and patterning defects. a** | Directing vorticial polar flows of bacteria dispersed in a nontoxic liquid crystal patterned with a periodic array of alternating ±1 defects (upper panel). The bacteria take counterclockwise trajectories around the defects (lower panel). **b** | A passive bulk smectic aligned by an external magnetic field couples hydrodynamically to an adjacent microtubule–kinesin active nematic film, forcing defects to orient and flow along alternating shear bands (scale bar: 100 µm). **c** | Patterning a tissue of human fibroblast cells (HDF) growing on a liquid crystal elastomer with a predesigned texture of ±1 defects (scale bars: 300 µm). **d** | Time series of dynamically assembled asters transported by local light activation along a predetermined trajectory within a bulk microtubule–kinesin suspension. Part **a** adapted with permission from REF.[135]. Part **b** adapted with permission from REF.[119]. Part **c** adapted with permission from REF.[138]. Part **d** adapted from REF.[75], Springer Nature Limited.

Another way to control the dynamics of active fluids is to confine them using curved substrates. Curvature frustrates order and often necessitates defects[13], providing a means of patterning active fluids. Nematics assembled onto spherical vesicles must accommodate a net topological charge of +2, as required by the Poincaré–Hopf theorem[20,129]. In equilibrium, for equal bend and splay elastic constants, the configuration lowest in energy corresponds to four +1/2 defects located at the corner of a tetrahedron inscribed by the sphere[130,131]. In active nematic vesicles, the four defects are motile and oscillate coherently between two equivalent tetrahedral configurations, driving spontaneous cell-like shape oscillations[64,98,132] (FIG. 1b). On a torus, the spatially varying positive and negative Gaussian curvature causes defects to unbind, attracting disclinations to regions of matching sign curvature[65], thereby filtering them by charge. On a sphere, polar fluids instead form vortices at the poles and a distinctive polar band that concentrates near the equator as a result of active advective fluxes pushing material towards the equator[133,134].

Experimental advances and defect-based control of active matter. A further challenge in controlling active matter is to engineer reconfigurable and programmable materials. A key strategy to this end is to use topological defects as natural motifs to build dynamic structures with organized flow. Biocompatible liquid crystals perfused with swimming bacteria afford simple static control through pre-patterned topological defects (FIG. 2a) that capture bacteria and direct their collective motion based on topological charge[135,136]. A related strategy has also been employed more recently to pattern defects in aligned epithelial monolayers (FIG. 2c) grown on structured substrates with strong anchoring[137,138].

Advances in optical control of biomolecular activity provide a platform to dynamically control and pattern active materials at will[75,76,139]. This has been demonstrated in microtubule–kinesin-based gels[75], in which local light activation reversibly self-assembles 3D asters that are dynamically stabilized by the clustering and polarized motion of motor proteins. These defect structures can be moved and arranged in arbitrary patterns in both space and time (FIG. 2d). A similar strategy has also been employed in active nematic films to locally pattern active stresses and direct defect motion using spatiotemporal activity gradients[76]. Inhomogeneous activity profiles can act as 'electric fields' that sort defects by topological charge[37], primarily owing to the self-propulsion of +1/2

Poincaré–Hopf theorem
A theorem in differential geometry and topology (also colloquially called the 'hairy ball theorem') that relates the number of zeros of a tangential vector field on a closed surface to the Euler characteristic of the same surface.

Bend and splay elastic constants
Material constants of a liquid crystal that quantify the energy cost of distorting orientational order through bend or splay deformations, respectively.

Morphogenesis
The process by which biological tissues, organs and organisms acquire their distinct shapes over the course of development.

Actomyosin
A complex of biopolymer filaments called actin, molecular motors called myosin and associated proteins. Actomyosin is commonly found in the cytoskeleton and cortex of cells, and is responsible for generating contraction, particularly in muscle.

Myoblasts
A type of embryonic stem cell that gives rise to muscle cells.

Mitotic spindle
A self-assembled cytoskeletal structure, consisting largely of stiff biopolymers called microtubules and a host of molecular motors and proteins, that plays a key role in eukaryotic cell division for segregating chromosomes to the two daughter cells.

Actin treadmilling
A dynamic process relevant to cell motility and crawling, by which cytoskeletal filaments such as actin get continually disassembled at one end, while monomer units are added at the other end.

Oocytes
Immature egg cells or germ cells involved in sexual reproduction.

Bulk gap
The region of frequency space where bulk modes do not exist.

disclinations that accumulate in regions of low activity, unlike non-motile −1/2 disclinations. This sorting can be exploited to create defect patterns in active fluids and concomitantly design functional materials with targeted transport capabilities. Defect-based control is poised to create innovative active metamaterials in the future[76,140], possibly facilitated by data-driven techniques[141–143].

Biological relevance of topological defects. An exciting development in active matter has been the characterization of topological defects in living tissues, bacterial colonies and even in multicellular organisms viewed as active materials. Elongated cells can form ordered liquid-crystalline textures interrupted by ±1/2 disclinations. In confluent epithelial tissues[71] and dense cultures of neural progenitors[72], cells preferentially migrate and accumulate at +1/2 disclinations and escape from −1/2 disclinations (FIG. 1e). This behaviour originates from the large distortion of order around the defect, which generates strong local active stresses (FIG. 1f). These large compressive stresses drive cell response and ultimately lead to cell extrusion and death in epithelia[71]. The structure and role of these active stresses have been confirmed by direct traction force microscopic measurements and by comparison with simulations of active nematic hydrodynamics. Similar phenomena have also been reported in bacterial systems. In growing biofilms, −1/2 defects instead provide sites for mound formation and buckling[79], and geometrically patterned +1 asters have been suggested to support verticalization[80]. Motile bacteria also display related behaviour: for instance, starved myxobacteria use ±1/2 defects to seed multilayers and cavities to initiate fruiting body formation[77], while slow-moving *Pseudomonas aeruginosa* cells outcompete faster mutants, as the latter form jams at defects, which hinders their ability to colonize space[78].

Another exciting frontier is the role of defects in organizing tissue morphogenesis. In the context of developing *Hydra*[73], topological defects in aligned supracellular actomyosin have been shown to correlate with specific morphogenetic processes in regenerating tissue. Remarkably, along with motile +1/2 disclinations, stable +1 defects emerge at locations that coincide with the eventual mouth and foot of the organism, thereby defining the body axis well before morphological features appear. In vitro experiments with confined myoblasts show tornado-like mound morphogenesis at patterned +1 asters that provide sites for growth and cellular differentiation[144,145]. Active defects also control the dynamic morphologies of growing cell layers[146], 2D bacterial colonies[147,148] and shape-shifting active shells[149]. General principles to unify these observations are not yet known, but these results suggest interesting ways in which active defects can constrain or be harnessed to serve diverse evolutionary, developmental and survival strategies.

On a subcellular level, the mitotic spindle exemplifies a self-organized aster-like defect maintained in constant flux by actin treadmilling and motor activity[150]. In a different example, in vivo experiments on starfish oocytes also demonstrate excitable biochemical spiral waves and defect chaos in the expression of certain membrane-bound signalling proteins[151]. Although the full implications of topological defects to biology remain to be seen, it is clear that this framework for studying biological systems is productive and at the frontier of active matter research.

Topological band structures in active matter

The topological defects discussed above are robust features of the order parameter of active media. We now turn to topologically protected waves, the robustness of which stems instead from their band structures. In general, a band structure describes the frequencies at which waves (such as sound modes) are allowed to propagate as a function of their wavevectors, along with the way the system vibrates at a given frequency. Frequency ranges in which waves are not allowed to propagate are called band gaps. As a simple example, consider a ring filled with air or any other fluid at rest. The clockwise and counterclockwise modes that correspond to density waves in the ring are degenerate, resulting in a point where the bands 'touch' in a lattice of such ring resonators. If a fan that circulates the air in a given direction is added to each ring, the degeneracy is broken (a bit like a spin in a magnetic field). As a result, a lattice of such circulators exhibits a band gap rather than a degeneracy[43,44].

The lattice of circulators exhibits two somewhat surprising properties characteristic of a class of materials called Chern insulators[15,16]. First, there are so-called edge states, which have frequencies in the bulk gap, the existence of which is guaranteed by topological invariants in the band structure. Second, these edge states propagate only along the boundaries of the material and — because the states arise from broken TRS — only in a single direction.

The construction of the topological invariants controlling this robust edge wave propagation can be intuited via a simple mathematical analogy. When the intrinsic (Gaussian) curvature of a toroid is integrated over the entire surface, the result must always equal zero, independent of the precise shape. This is an example of the Gauss–Bonnet theorem[129], which relates the integrated Gaussian curvature of a closed 2D surface to its genus. This powerful theorem makes it possible to calculate global topological features of a smooth surface from purely local geometric quantities. Analogously, the topological invariants of band structures are obtained by integrating an abstract curvature describing the geometry of eigenvalues and eigenvectors for the linear operator that governs wave propagation (BOX 2).

Here, we review the explanation for how topological band structures result in topologically protected modes at the boundary of a finite sample or at interfaces between systems with topologically distinct band structures. At an edge, the Chern number must go from its value in the bulk of the medium to zero (its value outside of the sample). This change cannot happen smoothly because the Chern number is an integer. Instead, the condition for defining a Chern number, namely, that the system is gapped, must cease to be valid at the edge, giving rise to confined wave propagation. The edge states resulting from this mechanism exhibit topological protection: they persist even if the properties of the medium are changed, as long as the bulk gap is not closed. As a consequence, the states exist even if defects, obstacles or sharp features

Box 2 | **Topological band theory in active fluids**

Upon linearization, the hydrodynamic models presented in TABLE 1 generically yield equations of the form

$$\partial_t \mathbf{X} = \mathbf{D}\mathbf{X},$$

where $\mathbf{D}$ is a matrix and $\mathbf{X}$ is a vector containing the departure of the hydrodynamic fields from their steady-state values (for instance, $\mathbf{X} = (\rho - \rho_0, \mathbf{u})$ combines the velocity field $\mathbf{u}$ and deviations of density ρ from steady-state value ρ_0 for a chiral active fluid with fixed rotation Ω). Equation (3) can be solved by performing a Fourier transform in space and time (that is, $\mathbf{X}(t, \mathbf{r}) \rightarrow \mathbf{X}\, e^{i(\omega t - \mathbf{q}\cdot\mathbf{r})}$). As an example, consider the spectrum of a chiral active fluid experiencing a Coriolis force $\mathbf{f}_B = \Omega_B \mathbf{u}_\perp$ that breaks time-reversal symmetry[168]

$$i\omega \begin{bmatrix} \rho/\rho_0 \\ u_x/c \\ u_y/c \end{bmatrix} = i \begin{bmatrix} 0 & q_x & q_y \\ q_x & 0 & -i(\Omega_B - \eta_o q^2) \\ q_y & i(\Omega_B - \eta_o q^2) & 0 \end{bmatrix} \begin{bmatrix} \rho/\rho_0 \\ u_x/c \\ u_y/c \end{bmatrix}, \quad (4)$$

where η_o denotes the odd viscosity coefficient discussed in the main text and TABLE 1. Diagonalizing $\mathbf{D}(\mathbf{q})$ in Eq. (4) yields its eigenvalues (plotted in black in part **a** of the figure), which, in turn, yield the dispersion relations $\omega_n(\mathbf{q})$ for band n. The associated eigenvectors $\mathbf{X}_n(\mathbf{q})$ can be used to determine the relevant topological invariant using a standard recipe (see REFS[17,255] for proofs and generalizations to systems with different spatial dimensions and symmetries).

First, calculate the so-called Berry connection $\mathcal{A}_n(\mathbf{q})$ from the eigenvectors (in a similar fashion to how one calculates the so-called spin connection of a surface[256]):

$$\mathcal{A}_n(\mathbf{q}) = i[\mathbf{X}_n(\mathbf{q})]^\dagger \cdot [\nabla_\mathbf{q} \mathbf{X}_n(\mathbf{q})]. \quad (5)$$

Second, determine the Berry curvature (as one would determine the Gaussian curvature from the spin connection[256]):

$$\mathcal{B}_n(\mathbf{q}) = \nabla_\mathbf{q} \times \mathcal{A}_n(\mathbf{q}). \quad (6)$$

Third, obtain the relevant topological invariants, called the first Chern numbers $\mathcal{C}_n$ (REF.[20]) (one per band) using a generalized Gauss–Bonnet formula. These topological indices can be seen as a generalization of the Euler characteristic of a surface[129,256], but with the Gaussian curvature replaced by the Berry curvature:

$$\mathcal{C}_n = \frac{1}{2\pi} \int d\mathbf{q}\, \mathcal{B}_n(\mathbf{q}). \quad (7)$$

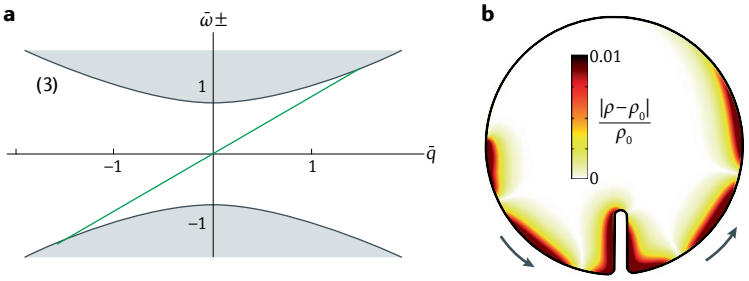

In the example discussed here, the first Chern number of the band with positive frequencies is[168]:

$$\mathcal{C}_+ = \text{sign}(\Omega_B) + \text{sign}(\eta_o). \quad (8)$$

The existence of non-vanishing first Chern numbers has striking physical consequences at the boundary of the system. In many cases, the algebraic number N of unidirectional modes with frequencies in the bulk band gap at an interface between two systems with Chern numbers $\mathcal{C}$ and $\mathcal{C}'$ is given by:

$$N = \mathcal{C} - \mathcal{C}'. \quad (9)$$

This relationship is called the bulk–boundary correspondence. Here, N is the number of modes propagating along the interface from left to right (or clockwise), minus the number of modes going from right to left (or counterclockwise). The band of these chiral edge states is shown as a green line (with positive slope) spanning the band gap in part **a** of the figure. One example of a specific edge state is shown in part **b** of the figure, which was obtained by driving the edge at a frequency within the band gap in a fluid dynamics simulation[168].

The Gauss–Bonnet formula directly gives the genus only of compact surfaces without boundary. Similarly, the first Chern numbers in Eq. (7) are defined only under certain conditions: the band n should be well separated from the others by band gaps, and momentum space should be compact. These conditions hold for fluids under periodic confinement[45] or subject to substrate curvature[134,167] but they are not generally guaranteed in fluids. As a consequence, the bulk–boundary correspondence does not always hold[168,171–174,176]. In our example, it is possible to compactify momentum space to get well-defined Chern numbers, as long as η_o is non-zero. When η_o vanishes, subtle effects can occur that require thinking outside of (this) box[168,171–174,176,178]!

Figure adapted with permission from REF.[168].

such as corners are present along the boundary. The waves propagate unabated through and around these obstructions without any backscattering: they cannot go back because the edge mode is unidirectional, and they cannot penetrate the gapped bulk.

Topological wave propagation is not unique to active media. Besides optical and quantum systems[15,30], it can also occur in mechanical systems, such as coupled oscillators[27,152,153] and simple fluids in circulator arrays[43,44]. Similar consequences ensue by harnessing active components to induce nontrivial band topology. As examples, a topological solid can be realized using ball-and-spring models with active feedback control[154,155] or by connecting motorized gyroscopes with springs[156–158]. The combination of the rotation of the gyroscopes and the geometry of the lattice breaks TRS and leads to a mechanical Chern insulator with chiral edge states at its boundary. These persist even when some of the gyroscopes are removed or immobilized. We illustrate the occurrence of topological waves in two classes of active fluids: polar active fluids composed of self-propelled particles and chiral active fluids composed of self-rotating particles.

Topological states in confined polar active fluids. Polar fluids naturally break TRS through spontaneous flows, which can be directed by geometric confinement to realize emergent chirality and topological edge states. We begin with the example of a polar active fluid confined in periodic microfluidic channels[45] (FIG. 3a–c). The channel geometry is composed of coupled rings, each reminiscent of an acoustic ring resonator[159] (FIG. 3d). Although the fluid itself is polar and achiral, because it is confined in a ring, the fluid has a spontaneously broken chiral symmetry, which distinguishes between clockwise and counterclockwise spontaneous flow[63,122,160,161].

Galilean invariance
The principle that constant boosts in velocity leave the system unchanged.

For a periodic geometry of rings on a square lattice[162], TRS is restored on average, because the neighbours of a clockwise ring must be counterclockwise and vice versa (in analogy with interlocking gears), so there is an equal number of clockwise and counterclockwise rings. By contrast, removing a single ring from a 2 × 2 supercell of the square lattice results in a so-called Lieb lattice, which has three rings per square unit cell in an L-shaped pattern (FIG. 3b). In this case, TRS is broken on the scale of the unit cell.

This difference between the square and Lieb lattices has drastic consequences for density waves. Owing to the presence of TRS, the square lattice has band crossings at certain symmetrical wavevectors. By contrast, TRS is broken in the Lieb lattice and band gaps open[45]. Each of these gapped bands indexed by n can be assigned a Chern number $\mathcal{C}_n$ (BOX 2), the value of which is generically non-zero, and is controlled by both the chirality of the flow and the geometry of the lattice. Note that, in other lattices (such as a honeycomb lattice), it is also possible to obtain topological states without a net unit cell vorticity[163] (FIG. 3c). In the limit in which the speed of flow v is smaller than the speed of sound c, the penetration depth for the localized mode scales as cd/v (where d is the lattice spacing), approaching d if $v \approx c$ (REF.[45]). In contrast to driven fluids[43,44], in which achieving this condition requires moderate Mach numbers or resonances, active fluids afford independent control of flow and sound speed, both of which are typically of the same order in experimental realizations[5,164]. As a result, active fluids host well-confined edge modes with penetration depth on the order of lattice spacing. This feature may be technologically advantageous in the design of miniaturized sonic waveguides[45,165,166].

Instead of periodic confinement, it is possible to use substrate curvature to produce topological edge states in polar active fluids[134] (FIG. 3e). Gaussian curvature coupled with mean flow breaks Galilean invariance and generically gaps long-wavelength sound modes that acquire a topological character owing to the absence of TRS. On the surface of a sphere, a polar active fluid spontaneously circulates around the equator in a chiral fashion[133,134], experiencing an active analogue of the Coriolis force that likewise changes sign across (and vanishes at) the equator. Passive fluids on a rotating sphere, common in geophysical and atmospheric contexts, also exhibit well-known equatorially localized topological sound modes[167] due to the inertial Coriolis force (FIG. 3f,g). In both cases, the equator acts as a gapless interface between two topologically distinct hemispheres. As a result, density waves in a polar active fluid on a spherical surface exhibit unidirectional propagation and topological protection along the equator, in addition to the polar fluid flows[134]. This phenomenon is generic to active flow on any surface with non-zero Gaussian curvature and leads to long-wavelength topological

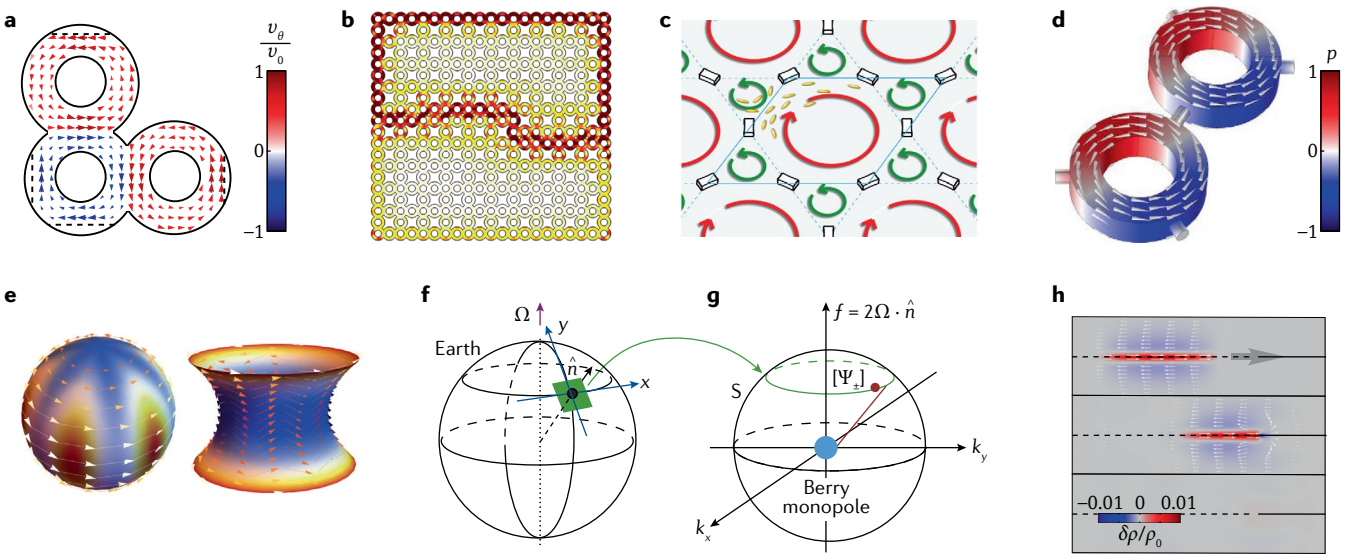

Fig. 3 | **Topological edge states in fluids far from equilibrium. a,b** | Phenomenology of topological edge states in a polar active fluid confined inside a Lieb lattice of annuli. Steady-state flow in terms of the azimuthal component of the velocity field v_θ normalized by the self-propulsion speed v_0 (part **a**) and topological density excitations at edges and interfaces of the lattice (part **b**) are shown. **c** | A polar active fluid with topological edge states but no net vorticity per unit cell. **d** | A topological material based on air driven within circulators, in which each unit cell has a net vorticity. Colour indicates the normalized pressure p. **e** | Topologically protected states arise at the equator in a polar active flock confined to the surface of a sphere (left) or a catenoid (right). **f,g** | Topological waves like those in part **e** arise on the scale of the Earth. The Earth has rotation vector Ω. At any point on its surface, the Coriolis parameter is $f = 2\Omega \cdot \hat{n}$, where $\hat{n}$ is the normal to the surface, and eigenmodes with wavefunction $\Psi_\pm$ are found in the space (k_x, k_y, f), where a sphere S surrounds the origin. The equator serves as a boundary along which geophysical waves are topologically protected by a Berry monopole that exists owing to the Earth's overall rotation. **h** | Boundary conditions that do not satisfy bulk–boundary correspondence can be exploited to create perfect absorption: a wavepacket of density excitation $\delta\rho$ around the steady-state density ρ_0 is sent in from the left (top); the wave is absorbed when it encounters a change in boundary conditions (middle), leading to the wavepacket being entirely absorbed (bottom). Parts **a** and **b** adapted from REF.[45], Springer Nature Limited. Part **c** adapted with permission from REF.[163]. Part **d** adapted from REF.[43]. Part **e** adapted with permission from REF.[134]. Parts **f** and **g** adapted with permission from REF.[167]. Part **h** adapted with permission from REF.[178].

Dynamical matrix
In the linear approximation, the dynamical matrix D_{ij} defines the potential energy V of a solid as the quadratic form $V=\frac{1}{2}\sum_{ij}u_iD_{ij}u_j$, where u_i are particle displacements and the i and j indices run over all dN degrees of freedom for an N-particle system in d dimensions.

Hermitian
A matrix $\mathbf{D}$ is Hermitian if $\mathbf{D}=\mathbf{D}^\dagger$. The † denotes a conjugate transpose, $(D^\dagger)_{ij}=D^*_{ji}$. A matrix $\mathbf{D}$ is anti-Hermitian if $\mathbf{D}=-\mathbf{D}^\dagger$.

Advection
The transport of matter and other quantities, such as momentum, temperature or concentration, by the bulk motion of a fluid.

sound modes localized along paths that are both geodesics and flow streamlines (FIG. 3e).

Topological waves and odd viscosity in chiral active fluids. In the above examples of polar active fluids, band-structure topology emerges from the spatial environment that the fluid inhabits. Activity primarily serves to break TRS, which, in turn, allows for non-zero Chern numbers. However, chiral active fluids exhibit topological states even in the absence of structured confinement[168] (BOX 2). In this case, activity itself endows the fluid with chirality and mesoscopic length scales, leading to topologically protected edge states.

For topological states in chiral fluids to exist, activity needs to simultaneously play two distinct roles: breaking TRS and creating a mesoscopic length scale in the fluid response. Consider a bulk chiral active fluid inside a disc. The fluid spontaneously rotates, owing to the balance between dissipation and the local torques arising from self-rotating constituents; over a broad parameter range, the preferred steady state is rigid-body rotation (having angular velocity Ω_B)[168–170] (BOX 1). This rigid-body rotation not only breaks TRS owing to the flow but also opens up a band gap around zero frequency in the fluid bulk. The origin of the band gap is, once again, rooted in the breaking of a basic symmetry of classical hydrodynamics: Galilean invariance. Rigid-body rotation breaks Galilean invariance by having a fixed rotation axis and leads to the presence of a band gap. Whereas polar fluids require confinement to generate rotation[45,63,122,134], chiral active fluids do so intrinsically in the bulk[168–170].

In fluids, the Chern number is not always well defined[168,171–174] (BOX 2), because the acoustic bands of a fluid are defined on the plane of wavevectors $\mathbf{q}$, which is a non-compact space. In contrast, in lattice systems, the wavevectors are only defined modulo reciprocal lattice vectors (they form a torus called the Brillouin zone, which is compact). In the example described in BOX 2, it is possible to replace the plane by a sphere because of the presence of a dissipationless viscosity called odd viscosity η_o (TABLE 1) that can act as a short-distance regularization[168,170,173,175,176]. A striking feature of chiral active fluids is that the Chern number in Eq. (7) in BOX 2 can change without closing the band gap. This jump occurs when η_o changes sign. The band gap does not close, because its width is determined solely by the rotation rate Ω_B, but the Chern number in Eq. (7) still changes. In this unusual topological phase transition, the hydrodynamic theory breaks down at short scales because the penetration depth of one of the edge modes goes to zero, and the transition can proceed without band inversion or band gap closure[168]. For the same reason, topological continuum theories also allow for violations of the bulk–boundary correspondence[168,171–174,176,177]. This violation can, in turn, be exploited to construct waveguides that perfectly absorb a mode in the presence of dissipation[178] (FIG. 3h). (A change in the Chern number without a band gap closing is also possible in polar active fluids on curved substrates, when the density and orientational sound speeds become equal, causing Galilean invariance to effectively be restored[134]. However, this mechanism is unrelated to any short-scale regularization.)

Non-Hermitian band theory in active media. So far in our discussion of topological band theory, we have tacitly assumed that the dynamical matrix $\mathbf{D}$ is Hermitian. When this assumption does not hold, the band structure can be literally more complex: the eigenvalues are neither purely real nor purely imaginary. The real parts correspond to the oscillation frequencies of the relevant perturbation and the imaginary parts correspond to the decay rates (or vice versa). In addition, we have also assumed that $\mathbf{D}$ is a normal operator, that is, $[\mathbf{D},\mathbf{D}^\dagger]=0$. This is always true if $\mathbf{D}$ is Hermitian. When this assumption does not hold, the eigenvectors of $\mathbf{D}$ need not be orthogonal to each other (BOX 3). Loosening these two assumptions requires generalizations of topological band theory[179–183]. An analogous relaxation of these assumptions exists in quantum mechanics, in which the Hamiltonian is Hermitian in a closed system, but need not be for open quantum systems. Two broad themes have been explored in non-Hermitian physics: non-Hermitian skin modes and exceptional points. Before providing an intuitive explanation of these concepts, we stress that their occurrence in classical systems is generic: there is no a priori reason why the linearized operator $\mathbf{D}$ should be Hermitian or even normal (BOX 3).

Consider, as a simple example, the advection–diffusion equation[184] that describes the transport of a dye with density ρ in a fluid with viscosity η and moving with constant velocity v_0:

$$\partial_t\rho=-v_0\partial_x\rho+\eta\partial_x^2\rho.$$

The Fourier-transformed dynamical matrix $\mathbf{D}(q_x)$ of this system is just a complex number given by $\mathbf{D}(q_x)=iv_0q_x-\eta q_x^2$ (where q_x is the wavevector). Manifestly, $\mathbf{D}(q_x)\neq\mathbf{D}^\dagger(q_x)$ because it has both real and imaginary parts. In this case, $\mathbf{D}(q_x)$ is normal but not Hermitian.

When a boundary is inserted in the fluid, the dye accumulates at one end because of the advection v_0. While hardly a surprising conclusion, this is, in fact, a very simple manifestation of the non-Hermitian skin effect: a general phenomenon in which the eigenmodes of a non-Hermitian operator are almost all localized to the edge of the system. An iconic example of non-Hermitian quantum mechanics is the so-called Hatano–Nelson model[181], which is essentially a quantum version of Eq. (2). From a classical perspective, the asymmetric hopping of electrons (leading to skin modes localized at the edge) in the Hatano–Nelson model can be simply thought of as a biased random walk: if the electrons are more likely to hop to the right than to the left, they accumulate at the right edge. As explained in BOX 3, the skin effect is characterized by a non-Hermitian winding number[185–187], a topological invariant distinct from the Chern number discussed in BOX 2.

In active media (FIG. 4a–c), various strategies have been devised to engineer the localization of energy using the non-Hermitian skin effect[179–183,186–200]. These approaches mostly rely on breaking a family of symmetries collectively

Box 3 | $\mathcal{PT}$ symmetry, exceptional points and skin modes in non-Hermitian band theory

In active systems, the dynamical matrix **D** is not always Hermitian (or even normal). Hence, its eigenvalues $s = \omega - i\sigma$ are not necessarily real: there can be a growth or decay rate σ in addition to the oscillation frequency ω. In general, the eigenvalues of **D** are real if and only if there is an antiunitary operator **O**, with $\mathbf{O}^2 = \mathbf{I}$ (where **I** is the identity matrix), that commutes with the dynamical matrix **D** and such that the eigenvectors ψ_i of **D** satisfy $\mathbf{O}\psi_i = \psi_i$. The operator **O** is a symmetry of the dynamical matrix, called generalized $\mathcal{PT}$ symmetry for historical reasons[182]. A situation can arise when **O** commutes with **D** while simultaneously $\mathbf{O}\psi_i \neq \psi_i$ for at least one of the eigenvectors of **D**. In this case, the (generalized) $\mathcal{PT}$ symmetry is said to be spontaneously broken (it is unbroken when $\mathbf{O}\psi_i = \psi_i$ for all i). The notion of $\mathcal{PT}$ symmetry can be thought of as a generalization of the statement that the eigenvalues of a real matrix must come in complex conjugate pairs. When all the eigenvalues are real, the $\mathcal{PT}$ symmetry is unbroken, otherwise, it is broken. To see this structure in a familiar context, consider the damped harmonic oscillator (part **a** of the figure) described by the non-normal matrix

$$\begin{bmatrix} \dot{p} \\ \dot{x} \end{bmatrix} = \begin{bmatrix} -\Gamma/M & -k \\ 1/M & 0 \end{bmatrix} \begin{bmatrix} p \\ x \end{bmatrix}, \tag{10}$$

where M is the mass, Γ the damping coefficient and k the spring constant. Transitions between $\mathcal{PT}$-unbroken and $\mathcal{PT}$-broken states are generically accompanied by exceptional points, where the two eigenvectors coalesce (red lines in part **b** of the figure). For the harmonic oscillator, the exceptional point occurs at critical damping, separating the overdamped and underdamped regimes.

An active example is given by a solid that has bonds that are described by the non-conservative force law $\mathbf{F}(\mathbf{r}) = -(k\hat{\boldsymbol{r}} + k^a\hat{\boldsymbol{\varphi}})\delta r$, where $\hat{\boldsymbol{r}}$ ($\hat{\boldsymbol{\varphi}}$) is a unit vector pointing along (transverse to) the bond vector, δr is the change in length of the bond, and k and k^a are spring constants (part **c** of the figure)[225]. When the bond is taken on a closed cycle, the work done $W = \oint \mathbf{F} \cdot \mathrm{d}\mathbf{r}$ is equal to k^a times the area enclosed by the path. The dynamical matrix that governs the motion of a single particle in the trap shown in part **d** of the figure exhibits an exceptional point at a critical value of $k^a/k = 1/\sqrt{3}$. Similar phenomena occur in overdamped solids made of non-conservative bonds whose linear evolution can be expressed through a non-normal dynamical matrix via

$$\Gamma \begin{bmatrix} \dot{u}_{\parallel} \\ \dot{u}_{\perp} \end{bmatrix} = q^2 \begin{bmatrix} B + \mu & K^o \\ -K^o - A & \mu \end{bmatrix} \begin{bmatrix} u_{\parallel} \\ u_{\perp} \end{bmatrix}. \tag{11}$$

Here, $u_{\parallel}(\mathbf{q})$ and $u_{\perp}(\mathbf{q})$ indicate the Fourier modes of the longitudinal and transverse displacement field. The coefficients B and μ are the bulk and shear moduli, while K^o and A are two additional active moduli[225] that exist in 2D isotropic media.

Exceptional points in $\mathcal{PT}$-symmetric systems generically mark the crossover between oscillating and strictly relaxing behaviours. In some cases, such as the active spring and simple harmonic oscillator, this transition can be readily visualized as a crossover between linear and circular motion[191]. The ability of non-Hermitian systems to host non-orthogonal eigenvectors gives rise to striking vibrational features, such as the non-Hermitian skin effect[188,191,199,254], as shown in part **e** of the figure. Unlike Hermitian topological edge modes, in which a subextensive number of modes are localized to the boundary, non-Hermitian systems exhibit skin modes that are extensive in number. Given a number λ in the complex plane, it is useful to introduce a winding number, $s(\lambda)$ (REFS[185,197]):

$$s(\lambda) \equiv \frac{1}{2\pi i} \int_0^{2\pi/d} \frac{\mathrm{d}}{\mathrm{d}q} \ln \det[D(q) - \lambda] \, \mathrm{d}q, \tag{12}$$

where d is the lattice spacing. When s is non-zero, a semi-infinite system will host a mode at the complex frequency λ localized at, say, the left or the right boundary, depending on the sign of s. In FIG. 4b, for instance, the frequency of a skin mode in an active beam (star) is encircled by the periodic boundary spectrum (solid line). The non-Hermitian invariant s distinguishes inequivalent paths in the complex eigenvalue plane, whereas the Chern number measures the winding of the eigenstates (BOX 2).

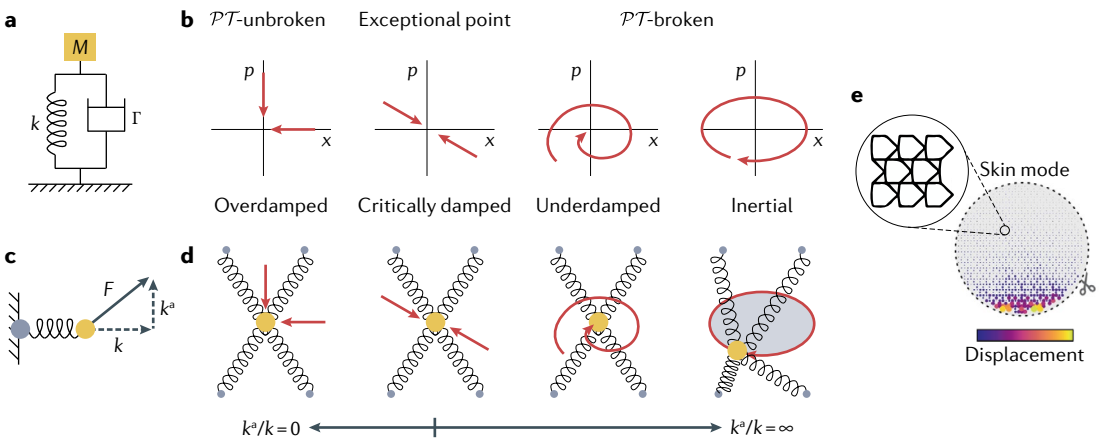

Figure part **e** adapted with permission from REF.[191].

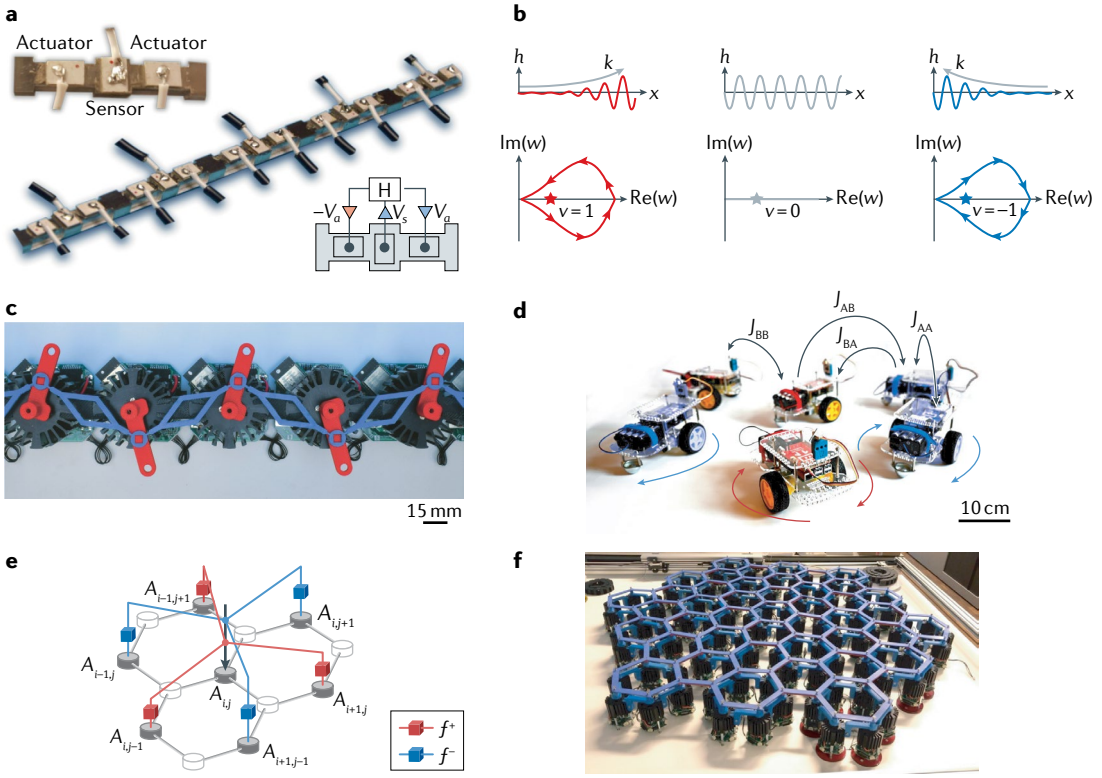

Fig. 4 | **Topology and exceptional points in active and robotic metamaterials. a** | Experimental realization of a self-sensing metabeam with active elasticity. A single unit cell featuring three piezoelectric patches: one that acts as a sensor and two that act as actuators. Each unit cell has an electronic feedback. **b** | Eigenmodes with open periodic boundary conditions with frequency corresponding to the star in the bottom panels. The localization of this eigenmode is determined by the sign of the winding of the energy in the complex plane. Sketches of the spectrum with periodic boundaries for each of the three cases: right localization, no localization and left localization. The arrows indicate directions of increasing wave number k. **c** | A robotic metamaterial composed of an array of sensors and motors (black, with red rods attached) coupled together by soft elastic beams (blue). The motors enforce non-reciprocal interactions in response to forces exerted by neighbours and detected using the sensors. The edge of this 1D metamaterial realizes modes corresponding to a non-Hermitian skin effect. Adapted from REF.[254]. **d** | A swarm of robots programmed to interact as non-reciprocal spins. Rather than aligning like a ferromagnet or anti-aligning like an antiferromagnet, the robots spontaneously rotate either clockwise or counterclockwise, despite having no average natural frequency and there being no external torque. The robotic spins are separated into two populations, A (blue) and B (red). The intraspecies exchange interactions J_{AA} and J_{BB} are reciprocal, but the interspecies interactions are not, with $J_{AB} \approx -J_{BA}$. **e** | A mechanical lattice with cells that are subject to active feedback forces processed through autonomous controllers. The A sites in cell $\{i,j\}$ are subject to active forces $f^{\pm}$ with either a positive or a negative relative phase. This system can be programmed to generate desired local response in real time, including topological edge states. **f** | A robotic metamaterial is built using a honeycomb lattice with robotic joints, the angular deflections of which are asymmetrically coupled. It exhibits an odd elastic modulus that couples the two shear modes (while maintaining conservation of both linear and angular momentum) and non-Hermitian skin modes. Parts **a** and **b** adapted from REF.[197]. Part **c** image courtesy of Martin Brandenbourger. Part **d** adapted from REF.[33], Springer Nature Limited. Part **e** adapted with permission from REF.[154]. Part **f** image courtesy of Corentin Coulais.

known as reciprocity[33,201–207]. For example, one approach[194] uses a 1D chain of coupled robots, the motors of which effectively violate Newton's third law and, therefore, break reciprocity (FIG. 4c). Similar effects have been observed in 1D microfluidic crystals[208] and other soft and active matter systems in which non-reciprocal interactions naturally emerge as a result of the particles being immersed in a medium or in contact with a substrate or field that provides linear or angular momentum[2,4,5,52,53,164,169,170,192,203–205,208–224]. In this case of non-reciprocal interactions, the presence of non-Hermitian skin modes can be explained using a simplified heuristic argument. Because the forces (or torques) at the two ends of a non-reciprocal bond are not equal and opposite, there is a net momentum flux across each bond. As a result, momentum or energy accumulates at one of the two ends of an open chain, as determined by the direction of the force (or torque) imbalance, much like the advected dye described by Eq. (2).

So far, we have explained how violations of linear and/or angular momentum conservation lead to non-reciprocity. Can one achieve similar effects (and the resulting non-Hermitian mechanical response) in a self-standing system not coupled to a substrate or any other momentum source or sink? The answer is yes — for example, when the system is active. To grasp this point, we need to consider a notion of reciprocity that is distinct from Newton's third law. This reciprocity, called

Maxwell–Betti reciprocity, can be intuitively defined as the symmetry between perturbation and response in a linear elastic solid. Consider an example in the context of Cauchy elasticity in which the deformation of a solid is described by a strain tensor u_{ij} and the internal forces by a stress tensor σ_{ij}. When a passive or active mechanical system is deformed, the infinitesimal work done is $\mathrm{d}W = \sigma_{ij}\mathrm{d}u_{ij}$. For small perturbations about an undeformed state, the stresses are related to strain deformations through $\sigma_{ij} = C_{ijkl}u_{kl}$, where C_{ijkl} is the tensor of elastic moduli. If the stress–strain relation can be derived from a free energy $V = \frac{1}{2}C_{ijkl}u_{ij}u_{kl}$, then C_{ijkl} is symmetric, that is, $C_{ijkl} = C_{klij}$. This symmetry is called Maxwell–Betti reciprocity[32].

When the microscopic forces are not conservative, Maxwell–Betti reciprocity is, in general, violated because $C_{ijkl} \neq C_{klij}$, and additional active elastic moduli are present, which we refer to as odd elasticity[225]. As a consequence, the dynamical matrix $D_{il}(\boldsymbol{q}) = C_{ijkl}q_jq_k$ that describes the propagation of elastic waves (BOX 3) is not Hermitian, allowing for the appearance of wave propagation in overdamped solids[225] and the presence of the skin effect[191]. Two example realizations of metamaterials with odd elasticity are an active metabeam with asymmetric coupling between shearing and bending[197] and a honeycomb lattice with robotic joints, the angular deflections of which are asymmetrically coupled (FIG. 4). In both systems, the skin effect has been observed. Its existence has also been inferred either from lattice models[192–194,226] or from continuum equations based only on symmetries and conservation laws[191,197]. Besides synthetic metamaterial or colloidal systems[197,227], odd elastic responses have recently been reported in living chiral crystals self-assembled from swimming starfish embryos[228].

So far, we have mostly focused on the eigenvalues of non-Hermitian dynamical matrices, but the corresponding eigenvectors play as crucial a role. When $\mathbf{D}$ is not normal, it is not always enough to know the eigenvalues to assess the linear stability of the system, because the eigenvectors can fail to be orthogonal to each other with respect to the physically relevant scalar product, for example, in a quadratic potential energy density. The extreme limit of this failure occurs when two (or more) eigenvectors become collinear: this is called an exceptional point[229]. As a consequence of this collinearity, there can be a transient amplification of perturbations that can dramatically affect the stability of the system[33,184,213,230–232]. A simple example of exceptional points occurs in the damped harmonic oscillator: the overdamped and underdamped regimes are separated by an exceptional point at critical damping (BOX 3). Likewise, in active metamaterials, odd elastic waves start propagating at the point where the eigenvalues of $\mathbf{D}$ go from being real (decay) to occurring in complex conjugate pairs (oscillations). This transition can be viewed as a spontaneous breaking of a symmetry called $\mathcal{PT}$ symmetry (BOX 3). When $\mathbf{D}$ is viewed as a differential operator in real space, its normality also depends on the boundary conditions. The skin effect occurs precisely when the eigenmodes of a system are orthogonal Fourier modes for a system with periodic boundaries, but become non-orthogonal localized modes in a semi-infinite or finite system. Exceptional points can also mediate unusual phase transitions in active many-body systems with non-reciprocal interactions[33,206,207].

Outlook

Open avenues for exploration remain when it comes to the relevance of topological properties of active systems to biology. Although defects in tissues have been noted as mechanically active centres of morphogenesis[71–73,77], current understanding of the interplay between active forcing and tissue response in manipulating cell organization is still limited. Integrating biologically relevant mechanisms such as growth, cell differentiation and mechanotransduction with the physics of active fluids would be crucial to this end. On a different scale, although biofilament–motor assemblies routinely display defects when reconstituted in vitro[7,40,55,233,234], the relation of these phenomena to in vivo cortical organization[150,151,235] remains mysterious and continues to be an open question. During development at the organ and organismal level, both collective motion and pattern formation are ubiquitous[236,237], offering an intriguing possibility for the realization of exotic, topologically protected states. There is also evidence of a role for topological states in non-equilibrium stochastic[238], excitable[239–242] and evolutionary dynamics[243] networks. One challenge faced by future theoretical work is the robustness of topological states to biologically relevant perturbations. In this regard, more systematic experimental investigations are needed.

Active metamaterials and synthetic active matter also offer a platform for engineering topological states, with an eye to applications[8,135]. Controlling and patterning defects using activity gradients has already emerged as a direction of research[37,75,76]. Whereas the focus so far has been on 2D systems, topological states in 3D offer new possibilities, including more complex defect textures[87] and topological degeneracies in band structure, such as Weyl nodes[244,245]. Designing synthetic gauge fields[45,115,246] and exceptional points in active fluids and solids[33,191,225] would be a powerful strategy to exploit these states for sensing and transport. Active flow is already being exploited, for example, to enhance in vitro fertilization[247,248], and creating topologically protected transport could be a route towards new technologies based on active matter.

From a theoretical perspective, important questions remain. Beyond topological band theory, the role of non-equilibrium noise and nonlinear interactions within active materials remains largely unexplored[33,206,207]. As discussed extensively, topological defects in active systems acquire much of their uniqueness from their dynamics[39]. Although much work has been done, a detailed understanding of defect-driven phase transitions and exotic defect-ordered states remains elusive. Towards this end, comparing and contrasting active defects with the collective dynamics of vortices in open quantum systems and driven dissipative condensates[249–251] promises to be a fruitful endeavour.

Published online 6 May 2022

Gauge fields
Terms that appear in the definition of an objective and covariant derivative (akin to the vector potential in electromagnetism) that capture how specific fields or order parameters transform under the action of local symmetries.

1. Ramaswamy, S. The mechanics and statistics of active matter. *Annu. Rev. Condens. Matter Phys.* **1**, 323–345 (2010).
2. Marchetti, M. C. et al. Hydrodynamics of soft active matter. *Rev. Mod. Phys.* **85**, 1143 (2013).
3. Ramaswamy, S. Active matter. *J. Stat. Mech. Theory Exp.* **2017**, 054002 (2017).
4. Palacci, J., Sacanna, S., Steinberg, A. P., Pine, D. J. & Chaikin, P. M. Living crystals of light-activated colloidal surfers. *Science* **339**, 936–940 (2013).
5. Bricard, A., Caussin, J.-B., Desreumaux, N., Dauchot, O. & Bartolo, D. Emergence of macroscopic directed motion in populations of motile colloids. *Nature* **503**, 95–98 (2013).
6. Schaller, V., Weber, C., Semmrich, C., Frey, E. & Bausch, A. R. Polar patterns of driven filaments. *Nature* **467**, 73–77 (2010).
7. Sanchez, T., Chen, D. T., DeCamp, S. J., Heymann, M. & Dogic, Z. Spontaneous motion in hierarchically assembled active matter. *Nature* **491**, 431–434 (2012).
8. Needleman, D. & Dogic, Z. Active matter at the interface between materials science and cell biology. *Nat. Rev. Mater.* **2**, 17048 (2017).
9. Cavagna, A. & Giardina, I. Bird flocks as condensed matter. *Annu. Rev. Condens. Matter Phys.* **5**, 183–207 (2014).
10. Trepat, X. & Sahai, E. Mesoscale physical principles of collective cell organization. *Nat. Phys.* **14**, 671–682 (2018).
11. Mermin, N. D. The topological theory of defects in ordered media. *Rev. Mod. Phys.* **51**, 591 (1979).
12. Alexander, G. P., Chen, B. G.-g, Matsumoto, E. A. & Kamien, R. D. Colloquium: Disclination loops, point defects, and all that in nematic liquid crystals. *Rev. Mod. Phys.* **84**, 497 (2012).
13. Nelson, D. R. *Defects and Geometry in Condensed Matter Physics* (Cambridge Univ. Press, 2002).
14. Kohmoto, M. Topological invariant and the quantization of the Hall conductance. *Ann. Phys.* **160**, 343–354 (1985).
15. Hasan, M. Z. & Kane, C. L. Colloquium: Topological insulators. *Rev. Mod. Phys.* **82**, 3045 (2010).
16. Qi, X.-L. & Zhang, S.-C. Topological insulators and superconductors. *Rev. Mod. Phys.* **83**, 1057 (2011).
17. Fruchart, M. & Carpentier, D. An introduction to topological insulators. *C. R. Phys.* **14**, 779 – 815 (2013).
18. Halperin, B. I. Quantized Hall conductance, current-carrying edge states, and the existence of extended states in a two-dimensional disordered potential. *Phys. Rev. B* **25**, 2185 (1982).
19. Moore, J. E. The birth of topological insulators. *Nature* **464**, 194–198 (2010).
20. Nakahara, M. *Geometry, Topology and Physics* (Taylor & Francis, 2003).
21. Ran, Y., Zhang, Y. & Vishwanath, A. One-dimensional topologically protected modes in topological insulators with lattice dislocations. *Nat. Phys.* **5**, 298–303 (2009).
22. Teo, J. C. & Kane, C. L. Topological defects and gapless modes in insulators and superconductors. *Phys. Rev. B* **82**, 115120 (2010).
23. Juričić, V., Mesaros, A., Slager, R.-J. & Zaanen, J. Universal probes of two-dimensional topological insulators: dislocation and π flux. *Phys. Rev. Lett.* **108**, 106403 (2012).
24. Paulose, J., Chen, B. G.-g & Vitelli, V. Topological modes bound to dislocations in mechanical metamaterials. *Nat. Phys.* **11**, 153–156 (2015).
25. Chaikin, P. M. & Lubensky, T. C. *Principles of Condensed Matter Physics* (Cambridge Univ. Press, 2000).
26. Zhang, X., Xiao, M., Cheng, Y., Lu, M.-H. & Christensen, J. Topological sound. *Commun. Phys.* **1**, 97 (2018).
27. Huber, S. D. Topological mechanics. *Nat. Phys.* **12**, 621–623 (2016).
28. Khanikaev, A. B. & Shvets, G. Two-dimensional topological photonics. *Nat. Photonics* **11**, 763–773 (2017).
29. Mao, X. & Lubensky, T. C. Maxwell lattices and topological mechanics. *Annu. Rev. Condens. Matter Phys.* **9**, 413–433 (2018).
30. Ozawa, T. et al. Topological photonics. *Rev. Mod. Phys.* **91**, 015006 (2019).
31. Ma, G., Xiao, M. & Chan, C. T. Topological phases in acoustic and mechanical systems. *Nat. Rev. Phys.* **1**, 281–294 (2019).
32. Nassar, H. et al. Nonreciprocity in acoustic and elastic materials. *Nat. Rev. Mater.* **5**, 667–685 (2020).
33. Fruchart, M., Hanai, R., Littlewood, P. B. & Vitelli, V. Non-reciprocal phase transitions. *Nature* **592**, 363–369 (2021).
34. Seifert, U. From stochastic thermodynamics to thermodynamic inference. *Annu. Rev. Condens. Matter Phys.* **10**, 171–192 (2019).
35. Gnesotto, F., Mura, F., Gladrow, J. & Broedersz, C. P. Broken detailed balance and non-equilibrium dynamics in living systems: a review. *Rep. Prog. Phys.* **81**, 066601 (2018).
36. Shankar, S., Ramaswamy, S., Marchetti, M. C. & Bowick, M. J. Defect unbinding in active nematics. *Phys. Rev. Lett.* **121**, 108002 (2018).
37. Shankar, S. & Marchetti, M. C. Hydrodynamics of active defects: from order to chaos to defect ordering. *Phys. Rev. X* **9**, 041047 (2019).
38. Ramaswamy, S., Simha, R. A. & Toner, J. Active nematics on a substrate: giant number fluctuations and long-time tails. *EPL* **62**, 196 (2003).
39. Doostmohammadi, A., Ignés-Mullol, J., Yeomans, J. M. & Saguës, F. Active nematics. *Nat. Commun.* **9**, 3246 (2018).
40. Kumar, N., Zhang, R., de Pablo, J. J. & Gardel, M. L. Tunable structure and dynamics of active liquid crystals. *Sci. Adv.* **4**, eaat7779 (2018).
41. Narayan, V., Ramaswamy, S. & Menon, N. Long-lived giant number fluctuations in a swarming granular nematic. *Science* **317**, 105–108 (2007).
Also see Supporting Information of this reference, page 4, same issue.
42. Giomi, L., Bowick, M. J., Ma, X. & Marchetti, M. C. Defect annihilation and proliferation in active nematics. *Phys. Rev. Lett.* **110**, 228101 (2013).
43. Khanikaev, A. B., Fleury, R., Mousavi, S. H. & Alu, A. Topologically robust sound propagation in an angular-momentum-biased graphene-like resonator lattice. *Nat. Commun.* **6**, 8260 (2015).
44. Yang, Z. et al. Topological acoustics. *Phys. Rev. Lett.* **114**, 114301 (2015).
45. Souslov, A., van Zuiden, B. C., Bartolo, D. & Vitelli, V. Topological sound in active-liquid metamaterials. *Nat. Phys.* **13**, 1091–1094 (2017).
46. Berezinskii, V. Destruction of long-range order in one-dimensional and two-dimensional systems having a continuous symmetry group i. classical systems. *Soviet J. Exp. Theor. Phys* **32**, 493–500 (1971).
47. Berezinskii, V. Destruction of long-range order in one-dimensional and two-dimensional systems possessing a continuous symmetry group. II. quantum systems. *Soviet J. Exp. Theor. Phys* **34**, 610–616 (1972).
48. Kosterlitz, J. M. & Thouless, D. J. Ordering, metastability and phase transitions in two-dimensional systems. *J. Phys. C Solid State Phys.* **6**, 1181 (1973).
49. Kosterlitz, J. The critical properties of the two-dimensional xy model. *J. Phys. C Solid State Phys.* **7**, 1046 (1974).
50. Kosterlitz, J. M. Kosterlitz–Thouless physics: a review of key issues. *Rep. Prog. Phys.* **79**, 026001 (2016).
51. Vicsek, T., Czirók, A., Ben-Jacob, E., Cohen, I. & Shochet, O. Novel type of phase transition in a system of self-driven particles. *Phys. Rev. Lett.* **75**, 1226–1229 (1995).
52. Toner, J. & Tu, Y. Long-range order in a two-dimensional dynamical xy model: how birds fly together. *Phys. Rev. Lett.* **75**, 4326 (1995).
53. Toner, J. & Tu, Y. Flocks, herds, and schools: a quantitative theory of flocking. *Phys. Rev. E* **58**, 4828 (1998).
54. Toner, J., Tu, Y. & Ramaswamy, S. Hydrodynamics and phases of flocks. *Ann. Phys.* **318**, 170–244 (2005).
55. Nédélec, F., Surrey, T., Maggs, A. C. & Leibler, S. Self-organization of microtubules and motors. *Nature* **389**, 305–308 (1997).
56. Surrey, T., Nédélec, F., Leibler, S. & Karsenti, E. Physical properties determining self-organization of motors and microtubules. *Science* **292**, 1167–1171 (2001).
57. Simha, R. A. & Ramaswamy, S. Hydrodynamic fluctuations and instabilities in ordered suspensions of self-propelled particles. *Phys. Rev. Lett.* **89**, 058101 (2002).
58. Voituriez, R., Joanny, J.-F. & Prost, J. Spontaneous flow transition in active polar gels. *EPL* **70**, 404 (2005).
59. Duclos, G. et al. Spontaneous shear flow in confined cellular nematics. *Nat. Phys.* **14**, 728–732 (2018).
60. Sumino, Y. et al. Large-scale vortex lattice emerging from collectively moving microtubules. *Nature* **483**, 448–452 (2012).
61. Schaller, V. & Bausch, A. R. Topological defects and density fluctuations in collectively moving systems. *Proc. Natl Acad. Sci. USA* **110**, 4488–4493 (2013).
62. Köster, D. V. et al. Actomyosin dynamics drive local membrane component organization in an in vitro active composite layer. *Proc. Natl Acad. Sci. USA* **113**, E1645–E1654 (2016).
63. Bricard, A. et al. Emergent vortices in populations of colloidal rollers. *Nat. Commun.* **6**, 7470 (2015).
64. Keber, F. C. et al. Topology and dynamics of active nematic vesicles. *Science* **345**, 1135–1139 (2014).
65. Ellis, P. W. et al. Curvature-induced defect unbinding and dynamics in active nematic toroids. *Nat. Phys.* **14**, 85–90 (2018).
66. Gruler, H., Dewald, U. & Eberhardt, M. Nematic liquid crystals formed by living amoeboid cells. *Eur. Phys. J. B* **11**, 187–192 (1999).
67. Kemkemer, R., Kling, D., Kaufmann, D. & Gruler, H. Elastic properties of nematoid arrangements formed by amoeboid cells. *Eur. Phys. J. E* **1**, 215–225 (2000).
68. Zhou, S., Sokolov, A., Lavrentovich, O. D. & Aranson, I. S. Living liquid crystals. *Proc. Natl Acad. Sci. USA* **111**, 1265–1270 (2014).
69. Duclos, G., Erlenkämper, C., Joanny, J.-F. & Silberzan, P. Topological defects in confined populations of spindle-shaped cells. *Nat. Phys.* **13**, 58–62 (2017).
70. Blanch-Mercader, C. et al. Turbulent dynamics of epithelial cell cultures. *Phys. Rev. Lett.* **120**, 208101 (2018).
71. Saw, T. B. et al. Topological defects in epithelia govern cell death and extrusion. *Nature* **544**, 212–216 (2017).
72. Kawaguchi, K., Kageyama, R. & Sano, M. Topological defects control collective dynamics in neural progenitor cell cultures. *Nature* **545**, 327–331 (2017).
73. Maroudas-Sacks, Y. et al. Topological defects in the nematic order of actin fibers as organization centers of *Hydra* morphogenesis. *Nat. Phys.* **17**, 251–259 (2021).
74. Giomi, L. Geometry and topology of turbulence in active nematics. *Phys. Rev. X* **5**, 031003 (2015).
75. Ross, T. D. et al. Controlling organization and forces in active matter through optically defined boundaries. *Nature* **572**, 224–229 (2019).
76. Zhang, R. et al. Spatiotemporal control of liquid crystal structure and dynamics through activity patterning. *Nat. Mater.* **20**, 875–882 (2021).
77. Copenhagen, K., Alert, R., Wingreen, N. S. & Shaevitz, J. W. Topological defects promote layer formation in *Myxococcus xanthus* colonies. *Nat. Phys.* **17**, 211–215 (2021).
78. Meacock, O. J., Doostmohammadi, A., Foster, K. R., Yeomans, J. M. & Durham, W. M. Bacteria solve the problem of crowding by moving slowly. *Nat. Phys.* **17**, 205–210 (2021).
79. Yaman, Y. I., Demir, E., Vetter, R. & Kocabas, A. Emergence of active nematics in chaining bacterial biofilms. *Nat. Commun.* **10**, 2285 (2019).
80. Basaran, M. et al. Large-scale orientational order in bacterial colonies during inward growth. *eLife* **11**, e72187 (2022).
81. Pismen, L. Dynamics of defects in an active nematic layer. *Phys. Rev. E* **88**, 050502 (2013).
82. Maitra, A. & Lenz, M. Spontaneous rotation can stabilise ordered chiral active fluids. *Nat. Commun.* **10**, 920 (2019).
83. Hoffmann, L. A., Schakenraad, K., Merks, R. M. & Giomi, L. Chiral stresses in nematic cell monolayers. *Soft Matter* **16**, 764–774 (2020).
84. Kruse, K., Joanny, J.-F., Jülicher, F., Prost, J. & Sekimoto, K. Asters, vortices, and rotating spirals in active gels of polar filaments. *Phys. Rev. Lett.* **92**, 078101 (2004).
85. Shendruk, T. N., Thijssen, K., Yeomans, J. M. & Doostmohammadi, A. Twist-induced crossover from two-dimensional to three-dimensional turbulence in active nematics. *Phys. Rev. E* **98**, 010601 (2018).
86. Čopar, S., Aplinc, J., Kos, Ž., Žumer, S. & Ravnik, M. Topology of three-dimensional active nematic turbulence confined to droplets. *Phys. Rev. X* **9**, 031051 (2019).
87. Duclos, G. et al. Topological structure and dynamics of three-dimensional active nematics. *Science* **367**, 1120–1124 (2020).
88. Binysh, J., Kos, Ž., Čopar, S., Ravnik, M. & Alexander, G. P. Three-dimensional active defect loops. *Phys. Rev. Lett.* **124**, 088001 (2020).
89. Whitfield, C. A. et al. Hydrodynamic instabilities in active cholesteric liquid crystals. *Eur. Phys. J. E* **40**, 50 (2017).
90. Metselaar, L., Doostmohammadi, A. & Yeomans, J. M. Topological states in chiral active matter: dynamic blue phases and active half-skyrmions. *J. Chem. Phys.* **150**, 064909 (2019).
91. Carenza, L. N., Gonnella, G., Marenduzzo, D. & Negro, G. Rotation and propulsion in 3D active chiral droplets. *Proc. Natl Acad. Sci. USA* **116**, 22065–22070 (2019).

92. Thampi, S. P., Golestanian, R. & Yeomans, J. M. Velocity correlations in an active nematic. *Phys. Rev. Lett.* **111**, 118101 (2013).
93. Wensink, H. H. et al. Meso-scale turbulence in living fluids. *Proc. Natl Acad. Sci. USA* **109**, 14308–14313 (2012).
94. Hemingway, E. J., Mishra, P., Marchetti, M. C. & Fielding, S. M. Correlation lengths in hydrodynamic models of active nematics. *Soft Matter* **12**, 7943–7952 (2016).
95. Guillamat, P., Ignés-Mullol, J. & Sagués, F. Taming active turbulence with patterned soft interfaces. *Nat. Commun.* **8**, 564 (2017).
96. Lemma, L. M., DeCamp, S. J., You, Z., Giomi, L. & Dogic, Z. Statistical properties of autonomous flows in 2D active nematics. *Soft Matter* **15**, 3264–3272 (2019).
97. Alert, R., Casademunt, J. & Joanny, J.-F. Active turbulence. *Annu. Rev. Condens. Matter Phys.* **13**, 143–170 (2022).
98. Khoromskaia, D. & Alexander, G. P. Vortex formation and dynamics of defects in active nematic shells. *New J. Phys.* **19**, 103043 (2017).
99. Cortese, D., Eggers, J. & Liverpool, T. B. Pair creation, motion, and annihilation of topological defects in two-dimensional nematic liquid crystals. *Phys. Rev. E* **97**, 022704 (2018).
100. Tang, X. & Selinger, J. V. Theory of defect motion in 2D passive and active nematic liquid crystals. *Soft Matter* **15**, 587–601 (2019).
101. Zhang, Y.-H., Deserno, M. & Tu, Z.-C. et al. Dynamics of active nematic defects on the surface of a sphere. *Phys. Rev. E* **102**, 012607 (2020).
102. Vafa, F., Bowick, M. J., Marchetti, M. C. & Shraiman, B. I. Multi-defect dynamics in active nematics. Preprint at *arXiv* 2007.02947 (2020).
103. Maitra, A., Lenz, M. & Voituriez, R. Chiral active hexatics: giant number fluctuations, waves, and destruction of order. *Phys. Rev. Lett.* **125**, 238005 (2020).
104. Angheluta, L., Chen, Z., Marchetti, M. C. & Bowick, M. J. The role of fluid flow in the dynamics of active nematic defects. *New J. Phys.* **23**, 033009 (2021).
105. Ambegaokar, V., Halperin, B., Nelson, D. R. & Siggia, E. D. Dynamics of superfluid films. *Phys. Rev. B* **21**, 1806 (1980).
106. Zippelius, A., Halperin, B. & Nelson, D. R. Dynamics of two-dimensional melting. *Phys. Rev. B* **22**, 2514 (1980).
107. DeCamp, S. J., Redner, G. S., Baskaran, A., Hagan, M. F. & Dogic, Z. Orientational order of motile defects in active nematics. *Nat. Mater.* **14**, 1110–1115 (2015).
108. Putzig, E., Redner, G. S., Baskaran, A. & Baskaran, A. Instabilities, defects, and defect ordering in an overdamped active nematic. *Soft Matter* **12**, 3854–3859 (2016).
109. Srivastava, P., Mishra, P. & Marchetti, M. C. Negative stiffness and modulated states in active nematics. *Soft Matter* **12**, 8214–8225 (2016).
110. Patelli, A., Djafer-Cherif, I., Aranson, I. S., Bertin, E. & Chaté, H. Understanding dense active nematics from microscopic models. *Phys. Rev. Lett.* **123**, 258001 (2019).
111. Doostmohammadi, A., Adamer, M. F., Thampi, S. P. & Yeomans, J. M. Stabilization of active matter by flow-vortex lattices and defect ordering. *Nat. Commun.* **7**, 10557 (2016).
112. Oza, A. U. & Dunkel, J. Antipolar ordering of topological defects in active liquid crystals. *New J. Phys.* **18**, 093006 (2016).
113. Pearce, D. J. G. et al. Orientational correlations in active and passive nematic defects. *Phys. Rev. Lett.* **127**, 197801 (2021).
114. Thijssen, K., Nejad, M. R. & Yeomans, J. M. Role of friction in multidefect ordering. *Phys. Rev. Lett.* **125**, 218004 (2020).
115. Chardac, A., Shankar, S., Marchetti, M. C. & Bartolo, D. Emergence of dynamic vortex glasses in disordered polar active fluids. *Proc. Natl Acad. Sci. USA* **118**, e2018218118 (2021).
116. Bechinger, C. et al. Active particles in complex and crowded environments. *Rev. Mod. Phys.* **88**, 045006 (2016).
117. Green, R., Toner, J. & Vitelli, V. Geometry of thresholdless active flow in nematic microfluidics. *Phys. Rev. Fluids* **2**, 104201 (2017).
118. Guillamat, P., Ignés-Mullol, J., Shankar, S., Marchetti, M. C. & Sagués, F. Probing the shear viscosity of an active nematic film. *Phys. Rev. E* **94**, 060602 (2016).
119. Guillamat, P., Ignés-Mullol, J. & Sagués, F. Control of active liquid crystals with a magnetic field. *Proc. Natl Acad. Sci. USA* **113**, 5498–5502 (2016).
120. Guillamat, P. et al. Active nematic emulsions. *Sci. Adv.* **4**, eaao1470 (2018).
121. Rajabi, M., Baza, H., Turiv, T. & Lavrentovich, O. D. Directional self-locomotion of active droplets enabled by nematic environment. *Nat. Phys.* **17**, 260–266 (2021).
122. Wioland, H., Woodhouse, F. G., Dunkel, J., Kessler, J. O. & Goldstein, R. E. Confinement stabilizes a bacterial suspension into a spiral vortex. *Phys. Rev. Lett.* **110**, 268102 (2013).
123. Lushi, E., Wioland, H. & Goldstein, R. E. Fluid flows created by swimming bacteria drive self-organization in confined suspensions. *Proc. Natl Acad. Sci. USA* **111**, 9733–9738 (2014).
124. Liu, S., Shankar, S., Marchetti, M. C. & Wu, Y. Viscoelastic control of spatiotemporal order in bacterial active matter. *Nature* **590**, 80–84 (2021).
125. Norton, M. M. et al. Insensitivity of active nematic liquid crystal dynamics to topological constraints. *Phys. Rev. E* **97**, 012702 (2018).
126. Opathalage, A. et al. Self-organized dynamics and the transition to turbulence of confined active nematics. *Proc. Natl Acad. Sci. USA* **116**, 4788–4797 (2019).
127. Shendruk, T. N., Doostmohammadi, A., Thijssen, K. & Yeomans, J. M. Dancing disclinations in confined active nematics. *Soft Matter* **13**, 3853–3862 (2017).
128. Hardoüin, J. et al. Reconfigurable flows and defect landscape of confined active nematics. *Commun. Phys.* **2**, 121 (2019).
129. Carmo, M. P. d. *Riemannian Geometry* (Birkhäuser, 1992).
130. Nelson, D. R. Toward a tetravalent chemistry of colloids. *Nano Lett.* **2**, 1125–1129 (2002).
131. Shin, H., Bowick, M. J. & Xing, X. Topological defects in spherical nematics. *Phys. Rev. Lett.* **101**, 037802 (2008).
132. Zhang, R., Zhou, Y., Rahimi, M. & De Pablo, J. J. Dynamic structure of active nematic shells. *Nat. Commun.* **7**, 13483 (2016).
133. Sknepnek, R. & Henkes, S. Active swarms on a sphere. *Phys. Rev. E* **91**, 022306 (2015).
134. Shankar, S., Bowick, M. J. & Marchetti, M. C. Topological sound and flocking on curved surfaces. *Phys. Rev. X* **7**, 031039 (2017).
135. Peng, C., Turiv, T., Guo, Y., Wei, Q.-H. & Lavrentovich, O. D. Command of active matter by topological defects and patterns. *Science* **354**, 882–885 (2016).
136. Genkin, M. M., Sokolov, A., Lavrentovich, O. D. & Aranson, I. S. Topological defects in a living nematic ensnare swimming bacteria. *Phys. Rev. X* **7**, 011029 (2017).
137. Endresen, K. D., Kim, M., Pittman, M., Chen, Y. & Serra, F. Topological defects of integer charge in cell monolayers. *Soft Matter* **17**, 5878–5887 (2021).
138. Turiv, T. et al. Topology control of human fibroblast cells monolayer by liquid crystal elastomer. *Sci. Adv.* **6**, eaaz6485 (2020).
139. Schuppler, M., Keber, F. C., Kröger, M. & Bausch, A. R. Boundaries steer the contraction of active gels. *Nat. Commun.* **7**, 13120 (2016).
140. Norton, M. M., Grover, P., Hagan, M. F. & Fraden, S. Optimal control of active nematics. *Phys. Rev. Lett.* **125**, 178005 (2020).
141. Li, H. et al. Data-driven quantitative modeling of bacterial active nematics. *Proc. Natl Acad. Sci. USA* **116**, 777–785 (2019).
142. Colen, J. et al. Machine learning active-nematic hydrodynamics. *Proc. Natl Acad. Sci. USA* **118**, e2016708118 (2021).
143. Zhou, Z. et al. Machine learning forecasting of active nematics. *Soft Matter* **17**, 738–747 (2021).
144. Guillamat, P., Blanch-Mercader, C., Kruse, K. & Roux, A. Integer topological defects organize stresses driving tissue morphogenesis. *Nat. Mater.* https://doi.org/10.1038/s41563-022-01194-5 (2022).
145. Blanch-Mercader, C., Guillamat, P., Roux, A. & Kruse, K. Quantifying material properties of cell monolayers by analyzing integer topological defects. *Phys. Rev. Lett.* **126**, 028101 (2021).
146. Comelles, J. et al. Epithelial colonies in vitro elongate through collective effects. *eLife* **10**, e57730 (2021).
147. Doostmohammadi, A., Thampi, S. P. & Yeomans, J. M. Defect-mediated morphologies in growing cell colonies. *Phys. Rev. Lett.* **117**, 048102 (2016).
148. Dell'Arciprete, D. et al. A growing bacterial colony in two dimensions as an active nematic. *Nat. Commun.* **9**, 4190 (2018).
149. Metselaar, L., Yeomans, J. M. & Doostmohammadi, A. Topology and morphology of self-deforming active shells. *Phys. Rev. Lett.* **123**, 208001 (2019).
150. Bruguës, J. & Needleman, D. Physical basis of spindle self-organization. *Proc. Natl Acad. Sci. USA* **111**, 18496–18500 (2014).
151. Tan, T. H. et al. Topological turbulence in the membrane of a living cell. *Nat. Phys.* **16**, 657–662 (2020).
152. Prodan, E. & Prodan, C. Topological phonon modes and their role in dynamic instability of microtubules. *Phys. Rev. Lett.* **103**, 248101 (2009).
153. Bertoldi, K., Vitelli, V., Christensen, J. & van Hecke, M. Flexible mechanical metamaterials. *Nat. Rev. Mater.* **2**, 17066 (2017).
154. Sirota, L., Ilan, R., Shokef, Y. & Lahini, Y. Non-Newtonian topological mechanical metamaterials using feedback control. *Phys. Rev. Lett.* **125**, 256802 (2020).
155. Sirota, L., Sabsovich, D., Lahini, Y., Ilan, R. & Shokef, Y. Real-time steering of curved sound beams in a feedback-based topological acoustic metamaterial. *Mech. Syst. Signal Process.* **153**, 107479 (2021).
156. Nash, L. M. et al. Topological mechanics of gyroscopic metamaterials. *Proc. Natl Acad. Sci. USA* **112**, 14495–14500 (2015).
157. Wang, P., Lu, L. & Bertoldi, K. Topological phononic crystals with one-way elastic edge waves. *Phys. Rev. Lett.* **115**, 104302 (2015).
158. Mitchell, N. P., Nash, L. M., Hexner, D., Turner, A. M. & Irvine, W. T. M. Amorphous topological insulators constructed from random point sets. *Nat. Phys.* **14**, 380–385 (2018).
159. Fleury, R., Sounas, D. L., Sieck, C. F., Haberman, M. R. & Alù, A. Sound isolation and giant linear nonreciprocity in a compact acoustic circulator. *Science* **343**, 516–519 (2014).
160. Stenhammar, J., Wittkowski, R., Marenduzzo, D. & Cates, M. E. Light-induced self-assembly of active rectification devices. *Sci. Adv.* **2**, e1501850 (2016).
161. Thampi, S. P., Doostmohammadi, A., Shendruk, T. N., Golestanian, R. & Yeomans, J. M. Active micromachines: microfluidics powered by mesoscale turbulence. *Sci. Adv.* **2**, e1501854 (2016).
162. Wioland, H., Woodhouse, F. G., Dunkel, J. & Goldstein, R. E. Ferromagnetic and antiferromagnetic order in bacterial vortex lattices. *Nat. Phys.* **12**, 341–345 (2016).
163. Sone, K. & Ashida, Y. Anomalous topological active matter. *Phys. Rev. Lett.* **123**, 205502 (2019).
164. Geyer, D., Morin, A. & Bartolo, D. Sounds and hydrodynamics of polar active fluids. *Nat. Mater.* **17**, 789–793 (2018).
165. Cha, J., Kim, K. W. & Daraio, C. Experimental realization of on-chip topological nanoelectromechanical metamaterials. *Nature* **564**, 229–233 (2018).
166. Cummer, S. A., Christensen, J. & Alù, A. Controlling sound with acoustic metamaterials. *Nat. Rev. Mater.* **1**, 16001 (2016).
167. Delplace, P., Marston, J. & Venaille, A. Topological origin of equatorial waves. *Science* **358**, 1075–1077 (2017).
168. Souslov, A., Dasbiswas, K., Fruchart, M., Vaikuntanathan, S. & Vitelli, V. Topological waves in fluids with odd viscosity. *Phys. Rev. Lett.* **122**, 128001 (2019).
169. van Zuiden, B. C., Paulose, J., Irvine, W. T., Bartolo, D. & Vitelli, V. Spatiotemporal order and emergent edge currents in active spinner materials. *Proc. Natl Acad. Sci. USA* **113**, 12919–12924 (2016).
170. Soni, V. et al. The odd free surface flows of a colloidal chiral fluid. *Nat. Phys.* **15**, 1188–1194 (2019).
171. Silveirinha, M. G. Proof of the bulk-edge correspondence through a link between topological photonics and fluctuation-electrodynamics. *Phys. Rev. X* **9**, 011037 (2019).
172. Volovik, G. An analog of the quantum Hall effect in a superfluid ^{3}He film. *Soviet Phys. JETP* **67**, 1804–1811 (1988).
173. Tauber, C., Delplace, P. & Venaille, A. Anomalous bulk-edge correspondence in continuous media. *Phys. Rev. Res.* **2**, 013147 (2020).
174. Tauber, C., Delplace, P. & Venaille, A. A bulk-interface correspondence for equatorial waves. *J. Fluid Mech.* **868**, R2 (2019).
175. Banerjee, D., Souslov, A., Abanov, A. G. & Vitelli, V. Odd viscosity in chiral active fluids. *Nat. Commun.* **8**, 1573 (2017).
176. Bal, G. Continuous bulk and interface description of topological insulators. *J. Math. Phys.* **60**, 081506 (2019).

177. Bal, G. Topological invariants for interface modes. Preprint at *arXiv* 1906.08345 (2019).
178. Baardink, G., Cassell, G., Neville, L., Milewski, P. A. & Souslov, A. Complete absorption of topologically protected waves. *Phys. Rev. E* **104**, 014603 (2021).
179. Budich, J. C., Carlström, J., Kunst, F. K. & Bergholtz, E. J. Symmetry-protected nodal phases in non-Hermitian systems. *Phys. Rev. B* **99**, 041406 (2019).
180. Ashida, Y., Gong, Z. & Ueda, M. Non-Hermitian physics. *Adv. Phys.* **69**, 249–435 (2020).
181. Hatano, N. & Nelson, D. R. Localization transitions in non-Hermitian quantum mechanics. *Phys. Rev. Lett.* **77**, 570–573 (1996).
182. Bender, C. M. & Boettcher, S. Real spectra in non-Hermitian Hamiltonians having PT symmetry. *Phys. Rev. Lett.* **80**, 5243–5246 (1998).
183. Bergholtz, E. J., Budich, J. C. & Kunst, F. K. Exceptional topology of non-Hermitian systems. *Rev. Mod. Phys.* **93**, 015005 (2021).
184. Trefethen, L. N. & Embree, M. *Spectra and Pseudospectra* (Princeton Univ. Press, 2005).
185. Gong, Z. et al. Topological phases of non-Hermitian systems. *Phys. Rev. X* **8**, 031079 (2018).
186. Zhang, K., Yang, Z. & Fang, C. Correspondence between winding numbers and skin modes in non-Hermitian systems. *Phys. Rev. Lett.* **125**, 126402 (2020).
187. Okuma, N., Kawabata, K., Shiozaki, K. & Sato, M. Topological origin of non-Hermitian skin effects. *Phys. Rev. Lett.* **124**, 086801 (2020).
188. Yao, S. & Wang, Z. Edge states and topological invariants of non-Hermitian systems. *Phys. Rev. Lett.* **121**, 086803 (2018).
189. Weidemann, S. et al. Topological funneling of light. *Science* **368**, 311–314 (2020).
190. Lee, C. H. & Thomale, R. Anatomy of skin modes and topology in non-Hermitian systems. *Phys. Rev. B* **99**, 201103 (2019).
191. Scheibner, C., Irvine, W. T. & Vitelli, V. Non-Hermitian band topology and skin modes in active elastic media. *Phys. Rev. Lett.* **125**, 118001 (2020).
192. Rosa, M. I. & Ruzzene, M. Dynamics and topology of non-Hermitian elastic lattices with non-local feedback control interactions. *New J. Phys.* **22**, 053004 (2020).
193. Zhou, D. & Zhang, J. Non-Hermitian topological metamaterials with odd elasticity. *Phys. Rev. Res.* **2**, 023173 (2020).
194. Ghatak, A., Brandenbourger, M., van Wezel, J. & Coulais, C. Observation of non-Hermitian topology and its bulk–edge correspondence in an active mechanical metamaterial. *Proc. Natl Acad. Sci. USA* **117**, 29561–29568 (2020).
195. Borgnia, D. S., Kruchkov, A. J. & Slager, R.-J. Non-Hermitian boundary modes and topology. *Phys. Rev. Lett.* **124**, 056802 (2020).
196. Schomerus, H. Nonreciprocal response theory of non-Hermitian mechanical metamaterials: response phase transition from the skin effect of zero modes. *Phys. Rev. Res.* **2**, 013058 (2020).
197. Chen, Y., Li, X., Scheibner, C., Vitelli, V. & Huang, G. Realization of active metamaterials with odd micropolar elasticity. *Nat. Commun.* **12**, 5935 (2021).
198. Tlusty, T. Exceptional topology in ordinary soft matter. *Phys. Rev. E* **104**, 025002 (2021).
199. Yamauchi, L., Hayata, T., Uwamichi, M., Ozawa, T. & Kawaguchi, K. Chirality-driven edge flow and non-Hermitian topology in active nematic cells. Preprint at *arXiv* 2008.10852 (2020).
200. Palacios, L. S. et al. Guided accumulation of active particles by topological design of a second-order skin effect. *Nat. Commun.* **12**, 4691 (2021).
201. Das, J., Rao, M. & Ramaswamy, S. Driven Heisenberg magnets: nonequilibrium criticality, spatiotemporal chaos and control. *EPL* **60**, 418–424 (2002).
202. Lahiri, R. & Ramaswamy, S. Are steadily moving crystals unstable? *Phys. Rev. Lett.* **79**, 1150–1153 (1997).
203. Uchida, N. & Golestanian, R. Synchronization and collective dynamics in a carpet of microfluidic rotors. *Phys. Rev. Lett.* **104**, 178103 (2010).
204. Saha, S., Ramaswamy, S. & Golestanian, R. Pairing, waltzing and scattering of chemotactic active colloids. *New J. Phys.* **21**, 063006 (2019).
205. Gupta, R. K., Kant, R., Soni, H., Sood, A. & Ramaswamy, S. Active nonreciprocal attraction between motile particles in an elastic medium. Preprint at *arXiv* 2007.04860 (2020).
206. You, Z., Baskaran, A. & Marchetti, M. C. Nonreciprocity as a generic route to traveling states. *Proc. Natl Acad. Sci. USA* **117**, 19767–19772 (2020).
207. Saha, S., Agudo-Canalejo, J. & Golestanian, R. Scalar active mixtures: the nonreciprocal Cahn-Hilliard model. *Phys. Rev. X* **10**, 041009 (2020).
208. Beatus, T., Tlusty, T. & Bar-Ziv, R. Phonons in a one-dimensional microfluidic crystal. *Nat. Phys.* **2**, 743–748 (2006).
209. Kumar, N., Soni, H., Ramaswamy, S. & Sood, A. Flocking at a distance in active granular matter. *Nat. Commun.* **5**, 4688 (2014).
210. Baek, Y., Solon, A. P., Xu, X., Nikola, N. & Kafri, Y. Generic long-range interactions between passive bodies in an active fluid. *Phys. Rev. Lett.* **120**, 058002 (2018).
211. Ivlev, A. V. et al. Statistical mechanics where Newton's third law is broken. *Phys. Rev. X* **5**, 011035 (2015).
212. Lavergne, F. A., Wendehenne, H., Bäuerle, T. & Bechinger, C. Group formation and cohesion of active particles with visual perception-dependent motility. *Science* **364**, 70–74 (2019).
213. Chajwa, R., Menon, N., Ramaswamy, S. & Govindarajan, R. Waves, algebraic growth, and clumping in sedimenting disk arrays. *Phys. Rev. X* **10**, 041016 (2020).
214. Kryuchkov, N. P., Ivlev, A. V. & Yurchenko, S. O. Dissipative phase transitions in systems with nonreciprocal effective interactions. *Soft Matter* **14**, 9720–9729 (2018).
215. Yifat, Y. et al. Reactive optical matter: light-induced motility in electrodynamically asymmetric nanoscale scatterers. *Light Sci. Appl.* **7**, 105 (2018).
216. Peterson, C. W., Parker, J., Rice, S. A. & Scherer, N. F. Controlling the dynamics and optical binding of nanoparticle homodimers with transverse phase gradients. *Nano Lett.* **19**, 897–903 (2019).
217. Morin, A., Caussin, J.-B., Eloy, C. & Bartolo, D. Collective motion with anticipation: flocking, spinning, and swarming. *Phys. Rev. E* **91**, 012134 (2015).
218. Dadhichi, L. P., Kethapelli, J., Chajwa, R., Ramaswamy, S. & Maitra, A. Nonmutual torques and the unimportance of motility for long-range order in two-dimensional flocks. *Phys. Rev. E* **101**, 052601 (2020).
219. Barberis, L. & Peruani, F. Large-scale patterns in a minimal cognitive flocking model: incidental leaders, nematic patterns, and aggregates. *Phys. Rev. Lett.* **117**, 248001 (2016).
220. Loos, S. A. M., Hermann, S. M. & Klapp, S. H. L. Non-reciprocal hidden degrees of freedom: a unifying perspective on memory, feedback, and activity. Preprinat at *arXiv* 1910.08372 (2019).
221. Bain, N. & Bartolo, D. Dynamic response and hydrodynamics of polarized crowds. *Science* **363**, 46–49 (2019).
222. Bertin, E., Droz, M. & Grégoire, G. Boltzmann and hydrodynamic description for self-propelled particles. *Phys. Rev. E* **74**, 022101 (2006).
223. Farrell, F. D. C., Marchetti, M. C., Marenduzzo, D. & Tailleur, J. Pattern formation in self-propelled particles with density-dependent motility. *Phys. Rev. Lett.* **108**, 248101 (2012).
224. Mishra, S., Baskaran, A. & Marchetti, M. C. Fluctuations and pattern formation in self-propelled particles. *Phys. Rev. E* **81**, 061916 (2010).
225. Scheibner, C. et al. Odd elasticity. *Nat. Phys.* **16**, 475–480 (2020).
226. Gao, P., Willatzen, M. & Christensen, J. Anomalous topological edge states in non-Hermitian piezophononic media. *Phys. Rev. Lett.* **125**, 206402 (2020).
227. Bililign, E. S. et al. Chiral crystals self-knead into whorls. *Nat. Phys.* **18**, 212–218 (2022).
228. Tan, T. H. et al. Development drives dynamics of living chiral crystals. Preprint at *arXiv* 2105.07507 (2021).
229. Heiss, W. The physics of exceptional points. *J. Phys. A* **45**, 444016 (2012).
230. Trefethen, L. N., Trefethen, A. E., Reddy, S. C. & Driscoll, T. A. Hydrodynamic stability without eigenvalues. *Science* **261**, 578–584 (1993).
231. Hanai, R. & Littlewood, P. B. Critical fluctuations at a many-body exceptional point. *Phys. Rev. Res.* **2**, 033018 (2020).
232. Strack, P. & Vitelli, V. Soft quantum vibrations of a PT-symmetric nonlinear ion chain. *Phys. Rev. A* **88**, 053408 (2013).
233. Edozie, B. et al. Self-organization of spindle-like microtubule structures. *Soft Matter* **15**, 4797–4807 (2019).
234. Weirich, K. L., Dasbiswas, K., Witten, T. A., Vaikuntanathan, S. & Gardel, M. L. Self-organizing motors divide active liquid droplets. *Proc. Natl Acad. Sci. USA* **116**, 11125–11130 (2019).
235. Gowrishankar, K. et al. Active remodeling of cortical actin regulates spatiotemporal organization of cell surface molecules. *Cell* **149**, 1353–1367 (2012).
236. Lecuit, T. & Mahadevan, L. Morphogenesis one century after on growth and form. *Development* **144**, 4197–4198 (2017).
237. Howard, J., Grill, S. W. & Bois, J. S. Turing's next steps: the mechanochemical basis of morphogenesis. *Nat. Rev. Mol. Cell Biol.* **12**, 392–398 (2011).
238. Murugan, A. & Vaikuntanathan, S. Topologically protected modes in non-equilibrium stochastic systems. *Nat. Commun.* **8**, 13881 (2017).
239. Kotwal, T. et al. Active topolectrical circuits. *Proc. Natl Acad. Sci. USA* **118**, e2106411118 (2021).
240. Hofmann, T., Helbig, T., Lee, C. H., Greiter, M. & Thomale, R. Chiral voltage propagation and calibration in a topolectrical Chern circuit. *Phys. Rev. Lett.* **122**, 247702 (2019).
241. Helbig, T. et al. Generalized bulk–boundary correspondence in non-Hermitian topolectrical circuits. *Nat. Phys.* **16**, 747–750 (2020).
242. Ronellenfitsch, H. & Dunkel, J. in *2020 Fourteenth International Congress on Artificial Materials for Novel Wave Phenomena (Metamaterials)* 270–272 (IEEE, 2020).
243. Knebel, J., Geiger, P. M. & Frey, E. Topological phase transition in coupled rock-paper-scissors cycles. *Phys. Rev. Lett.* **125**, 258301 (2020).
244. Armitage, N., Mele, E. & Vishwanath, A. Weyl and Dirac semimetals in three-dimensional solids. *Rev. Mod. Phys.* **90**, 015001 (2018).
245. Fruchart, M. et al. Soft self-assembly of Weyl materials for light and sound. *Proc. Natl Acad. Sci. USA* **115**, E3655–E3664 (2018).
246. Abbaszadeh, H., Souslov, A., Paulose, J., Schomerus, H. & Vitelli, V. Sonic Landau levels and synthetic gauge fields in mechanical metamaterials. *Phys. Rev. Lett.* **119**, 195502 (2017).
247. Denissenko, P., Kantsler, V., Smith, D. J. & Kirkman-Brown, J. Human spermatozoa migration in microchannels reveals boundary-following navigation. *Proc. Natl Acad. Sci. USA* **109**, 8007–8010 (2012).
248. Kantsler, V., Dunkel, J., Blayney, M. & Goldstein, R. E. Rheotaxis facilitates upstream navigation of mammalian sperm cells. *eLife* **3**, e02403 (2014).
249. Altman, E., Sieberer, L. M., Chen, L., Diehl, S. & Toner, J. Two-dimensional superfluidity of exciton polaritons requires strong anisotropy. *Phys. Rev. X* **5**, 011017 (2015).
250. Alicea, J., Balents, L., Fisher, M. P., Paramekanti, A. & Radzihovsky, L. Transition to zero resistance in a two-dimensional electron gas driven with microwaves. *Phys. Rev. B* **71**, 235322 (2005).
251. Wachtel, G., Sieberer, L., Diehl, S. & Altman, E. Electrodynamic duality and vortex unbinding in driven-dissipative condensates. *Phys. Rev. B* **94**, 104520 (2016).
252. Marchetti, M. C., Fily, Y., Henkes, S., Patch, A. & Yllanes, D. Minimal model of active colloids highlights the role of mechanical interactions in controlling the emergent behavior of active matter. *Curr. Opin. Colloid Interface Sci.* **21**, 34–43 (2016).
253. Cates, M. E. & Tailleur, J. Motility-induced phase separation. *Annu. Rev. Condens. Matter Phys.* **6**, 219–244 (2015).
254. Brandenbourger, M., Locsin, X., Lerner, E. & Coulais, C. Non-reciprocal robotic metamaterials. *Nat. Commun.* **10**, 4608 (2019).
255. Asbóth, J. K., Oroszlány, L. & Pályi, A. *A Short Course on Topological Insulators* (Springer, 2016).
256. Kamien, R. D. The geometry of soft materials: a primer. *Rev. Mod. Phys.* **74**, 953 (2002).

Acknowledgements

The work of M.J.B. was supported in part by the National Science Foundation under grant no. NSF PHY-1748958 and the Designing Materials to Revolutionize and Engineer our Future (DMREF) programme, via grant no. DMREF-1435794. M.C.M. was primarily supported by the National Science Foundation under grant no. DMR-2041459, with additional support from DMR-1720256 (iSuperSeed). S.S. is supported by the Harvard Society of Fellows. V.V. was supported by the Complex Dynamics and Systems programme of the Army Research Office under grant W911NF-19-1-0268, by the Simons Foundation and by the University of Chicago Materials Research Science and Engineering Center, which is funded by the National Science Foundation under award number DMR-2011854. S.S. and A.S. gratefully acknowledge discussions during the 2019 summer workshop on 'Active and Driven Matter: Connecting Quantum and Classical

Systems' at the Aspen Center for Physics, which is supported by National Science Foundation grant PHY-1607611. The participation of A.S. at the Aspen Center for Physics was supported by the Simons Foundation. A.S. acknowledges the support of the Engineering and Physical Sciences Research Council (EPSRC) through New Investigator Award no. EP/T000961/1 and of the Royal Society under grant no. RGS/R2/202135. The authors also acknowledge illuminating discussions throughout the virtual 2020 KITP programme on 'Symmetry, Thermodynamics and Topology in Active Matter', which was supported in part by the National Science Foundation under grant no. NSF PHY-1748958. The authors thank M. Fruchart, C. Scheibner, G. Baardink and J. Binysh for their inspiring conversations and suggestions.

Author contributions
All authors contributed equally to this article.

Competing interests
The authors declare no competing interests.

Peer review information
Nature Reviews Physics thanks Oleg Lavrentovich, Amin Doostmohammadi and the other, anonymous, reviewer(s) for their contribution to the peer review of this work.

Publisher's note
Springer Nature remains neutral with regard to jurisdictional claims in published maps and institutional affiliations.